

Nikolaus Rauch, BSc

**Optimization of sensitivity factor ( $\zeta$ -factor)  
measurements  
for quantitative X-ray spectrometry  
in the TEM**

**MASTER'S THESIS**

to achieve the university degree of  
Diplom-Ingenieur  
Master's degree programme: Advanced Material Science

submitted to

**Graz University of Technology**

**Supervisor**

Ao. Univ.-Prof. Dipl.-Ing. Dr. techn Werner Grogger

**Co-Supervisor**

Dipl.-Ing. Judith Lammer

Institute of Electron Microscopy  
and Nanoanalysis

Graz, June 2020



---

## Affidavit

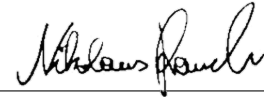
---

I declare that I have authored this thesis independently, that I have not used other than the declared sources/resources, and that I have explicitly indicated all material which has been quoted either literally or by content from the sources used. The text document uploaded to TUGRAZonline is identical to the present master's thesis.

17.06.2020

---

Date



---

Signature



---

## Kurzfassung

---

Es gibt zwei etablierte Methoden zur EDX-Quantifizierung im Transmissionselektronenmikroskop: die konventionelle Cliff-Lorimer- und die neuere  $\zeta$ -Faktor-Methode. Mit der  $\zeta$ -Faktor-Methode ist es nicht nur möglich, die Konzentration der einzelnen Elemente zu bestimmen, sondern auch die Massendicke der betrachteten Probenstelle. Damit ist eine Absorptionskorrektur bei leichten Elementen einfach durchführbar. Die Voraussetzung für diese Technik ist die Verfügbarkeit von Empfindlichkeitsfaktoren ( $\zeta$ -Faktoren). Es ist jedoch schwierig, genaue Werte für leichte Elemente zu bestimmen, was zu unzuverlässigen Quantifizierungsergebnissen führt.

In dieser Arbeit werden einige Ansätze zur Bestimmung von  $\zeta$ -Faktoren diskutiert sowie ein komplett neuer entwickelt. Hierzu wird der Effekt der Röntgenabsorption genutzt und damit die üblicherweise notwendige Dickenmessung umgangen. Die Daten, die für die experimentelle Bestimmung von  $\zeta$ -Faktoren notwendig sind, wurden mittels EDXS und EELS ermittelt.

Mit Hilfe sogenannter Horita-Plots kann der exponentielle Verlauf der teilweise absorbierten Röntgenlinien indirekt in Abhängigkeit von der Probendicke dargestellt werden. Exponentielle Fits aus den Plots ermöglichen die Bestimmung genauer  $\zeta$ -Faktoren speziell für leichte Elemente, welche in dieser Arbeit für Kohlenstoff und Sauerstoff bestimmt wurden.



---

## Abstract

---

There are two common methods for elemental quantification via EDXS in the TEM: the conventional Cliff-Lorimer technique and the newer  $\zeta$ -factor method. Using the  $\zeta$ -factor method, one can not only obtain the elemental concentrations but also the mass-thickness of the observed specimen area. Thereby, a proper absorption correction for light elements is possible. A precondition for using this method is the determination of sensitivity factors ( $\zeta$ -factors). However, it is hard to get accurate values for light elements which makes the quantification of such highly unreliable.

In this work, several known approaches to determine  $\zeta$ -factors are discussed and a completely new one is developed which uses the effect of absorption of low-energy X-rays within the specimen. Therefore, no thickness measurement is necessary anymore. The required data to determine  $\zeta$ -factors experimentally was obtained by simultaneously acquired EDXS and EELS Spectrum Images.

Via so-called Horita-Plots, the exponential behavior of the partly absorbed X-ray lines is indirectly depicted in dependence of the specimen thickness. Exponential fits from these plots allow the determination of accurate  $\zeta$ -factors, especially for light elements which, in this thesis, were determined for carbon and oxygen.





---

## Acknowledgements

---

At this point I would like to acknowledge all people who made this work possible and supported me.

I want to thank my supervisors Werner Grogger for his remarkable support and scientific guidance through my whole work as well as Ferdinand Hofer the head of the institute. A special thank you goes to my co-supervisor Judith Lammer for her tremendous commitment, for sharing her time measuring with me at the microscopes and for many fruitful discussions and advises. I express my gratitude to Martina Dienstleder and Sebastian Rauch for their accurate specimen preparation.

Moreover, I would like to thank my colleagues in the master's office Alex, Benni, Jakob, Michi, Moritz and Verena as well as the TEM-group and the entire FELMI-ZFE team for the pleasant working atmosphere and light-hearted coffee breaks.

Last but not least, I would like to thank my family, my friends and my girlfriend Christiane who supported me during this thesis and through all my studies.



---

## Contents

---

<b>1</b>	<b>Introduction</b>	<b>1</b>
<b>2</b>	<b>Fundamentals of EDXS in the TEM</b>	<b>3</b>
2.1	Generation of X-rays . . . . .	3
2.2	Absorption of X-rays . . . . .	5
2.3	Quantitative X-ray analysis . . . . .	6
2.3.1	The Cliff-Lorimer method . . . . .	6
2.3.2	The $\zeta$ -factor method . . . . .	7
2.4	Extrapolation methods - new approaches for $\zeta$ -factor determination . . . . .	11
2.4.1	Horita plots . . . . .	11
2.4.2	Method <b>A</b> - Thickness dependence of $k_{AB}$ -factor . . . . .	13
2.4.3	Method <b>B</b> - Intensity dependence of reference intensity . . . . .	14
2.4.4	Method <b>C</b> - Intensity dependence of $\frac{t}{\lambda}$ . . . . .	15
<b>3</b>	<b>Experiments and results</b>	<b>19</b>
3.1	Specimens . . . . .	19
3.1.1	Choice of samples . . . . .	19
3.1.2	Specimen preparation . . . . .	21
3.2	Used TEM-EDXS system . . . . .	21
3.3	Acquisition of required data . . . . .	23
3.3.1	Determining peak intensities of EDX spectra . . . . .	24
3.3.2	Determination of $\frac{t}{\lambda}$ -values . . . . .	24
3.4	$\zeta$ -factor determination . . . . .	25
3.5	Results . . . . .	30
<b>4</b>	<b>Conclusion</b>	<b>41</b>
	<b>Bibliography</b>	<b>43</b>
	<b>Appendix</b>	<b>51</b>
<b>A</b>	<b>Used Matlab scripts</b>	<b>51</b>
A.1	Matlab script to evaluate EDX-spectra in terms of peak intensities . . . . .	51
A.2	Matlab script to quantify EDX-spectra using the $\zeta$ -factor method . . . . .	57

<b>B Additional graphs</b>	<b>61</b>
B.1 Residual graphs for $\zeta$ -factor determination . . . . .	61
B.2 Residual graphs of the quantification-procedure via the $\zeta$ -factor method . . .	65
<b>C Error analysis</b>	<b>69</b>

# CHAPTER 1

---

## Introduction

---

State-of-the-art transmission electron microscopes (TEM) reach resolutions smaller than 100 pm. Considering the lengths of atomic distances (on the order of a few tenths of a nanometer), it is possible to image and detect lattice defects, grain boundaries and even single atoms of a solid. Most TEMs are used as analytical electron microscopes (AEM) which means that - additional to imaging methods - the chemical composition of a specimen can be investigated. The combination of good lateral resolution and precise chemical analytical capabilities is the reason why the TEM is such a powerful instrument. The investigation of very small features and the ability to tell what they are made of are often the key for further conclusions. Two main techniques for chemical analysis in the TEM are energy-dispersive X-ray spectroscopy (EDXS) and electron energy loss spectroscopy (EELS).

If an atom within the specimen is ionized by the primary electron beam, it may emit a characteristic X-ray when it returns to its ground state. This X-ray is characteristic for a specific element and gets evaluated by the EDXS system to provide qualitative and quantitative information about the specimen. This technique has been usually used for the detection of middle and heavy elements, whereas light elements are more challenging due to small detector efficiencies and fluorescence yields for low energy X-rays. Moreover, the lower the energy of an X-ray is, the more likely it gets absorbed by the specimen itself and is no longer detectable. Nevertheless, with modern EDXS systems it is nowadays possible to detect elements down to beryllium. Contrary to the qualitative analysis, the quantification of light elements with EDXS is still a major issue to overcome.

The  $\zeta$ -factor is one method to evaluate X-ray spectra quantitatively [1]. It requires the respective peak intensities, the electron dose and the element and microscope specific  $\zeta$ -factors. However, for the determination of such  $\zeta$ -factors, the specimens thickness of the sample has to be known. Since accurate thickness measurements at the nanometer scale are not trivial at all and hard to perform, the aim of this work is to develop a method to determine  $\zeta$ -factors without the necessity of knowing the specimen's thickness. The idea is to harness the effect of X-ray absorption within the specimen which is thickness-dependent and to calculate  $\zeta$ -factors from this information. This is a promising approach especially for light elements whose characteristic X-ray lines substantially suffer from absorption which is usually a major drawback for the analysis of such, but in this case is used to our advantage.



# CHAPTER 2

## Fundamentals of EDXS in the TEM

The method developed in this thesis is based on the generation and absorption of X-rays. Therefore, these effects as well as the predominant EDXS quantification methods are discussed.

### 2.1 Generation of X-rays

X-rays can be categorized into two sections based on their production - characteristic X-rays and bremsstrahlung. While characteristic X-rays are used for qualitative and quantitative analysis, bremsstrahlung is generally unwanted and has to be considered as a background signal. If a high-energy electron interacts with inner-shell electrons, an ionization process may occur. If an inner-shell electron is kicked out of the atom and escapes the attractive field of the nucleus, the atom is left in an excited state because it has an excess of energy, and we describe it as ionized. To return to the ground state, the generated hole is filled with an electron from an outer shell. Along with this transition, either an X-ray or an Auger electron with a specific energy is emitted. [2]

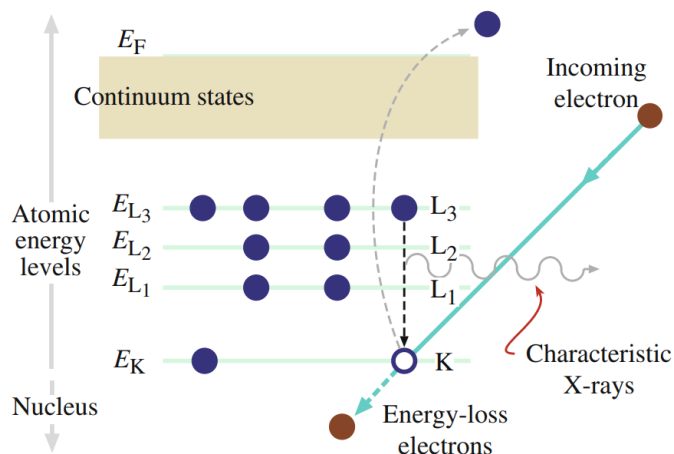


**Figure 2.1:** The ionization process. An inner (K) shell electron is ejected from the atom by a high-energy electron. When the hole in the K-shell is filled by an electron from the L-shell, characteristic ( $K\alpha$ ) X-ray emission occurs. The incident electron loses energy and continues its way through the specimen. (taken from D. B. Williams et al. [2])

The energy of characteristic X-rays depends on the difference of the participating shell

energies during the ionization and the relaxation process. Since every element has unique energy levels, each detected energy can be assigned to an individual element. The more shells an atom has, i.e. the heavier it is, the more possibilities for different transitions exist with simultaneous consideration of Fermi's golden rule. Oxygen, for example, has only one characteristic X-ray main line at 0.523 keV, whereas zinc has two main lines at 8.637 keV and 1.012 keV. Moreover, each shell consists of further sub-shells resulting in sub-peaks with similar energies as the main specific X-ray line.

In figure 2.2 possible kinds of transitions are shown. The nomenclature of the different shells is K, L, M, N, O and is called Siegbahn notation. The X-ray line of a transition from a higher shell to the K-shell is called K-line, to the L-shell L-line and to the M-shell M-line. Depending on the shell and sub-shell where the electron came from, the numerated suffixes such as  $\alpha$ ,  $\beta$ ,  $\gamma$  and  $\delta$  are used.

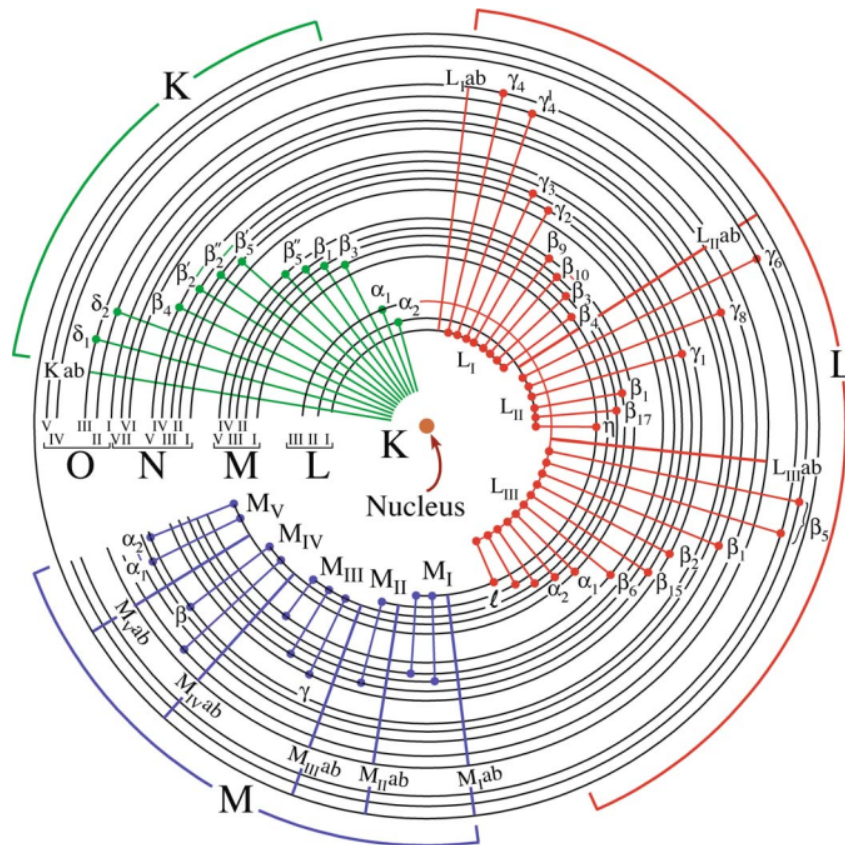


**Figure 2.2:** Possible electron transitions that give rise to K, L and M characteristic X-rays. Not all of them are detectable by the EDXS in the TEM. (taken from D. B. Williams et al. [2])

If an electron interacts inelastically with the nucleus, it experiences a change in momentum by interacting with the nucleus' Coulomb field. During this process, an X-ray which



gives rise to the above-mentioned bremsstrahlung may be emitted. The energy of the emitted X-rays is dependent on the incident beam energy and the atomic number  $Z$  of the ionized atom. Unwanted bremsstrahlung adulterates the intensities of the characteristic X-ray peaks and, therefore, has to be subtracted from the spectrum.

## 2.2 Absorption of X-rays

The absorption of characteristic X-rays within the specimen is a major issue for quantification. If X-rays are absorbed, they will not be detected. Therefore, the measured intensities are falsified and need to be corrected. To understand the methods used in this work, a brief insight into the theory of the absorption effect is given.

The mass attenuation coefficient  $\mu/\rho$

The mass attenuation coefficient (MAC) is the quotient of the linear attenuation coefficient and the density of a material. It expresses how much electromagnetic radiation is damped by passing through matter depending on the photon's energy. The exponential decay of the initial intensity is described by the Beer-Lambert law. [3]

$$I = I_0 \cdot e^{(-\frac{\mu}{\rho}\rho d)} \quad (2.1)$$

$I$ ...intensity of the transmitted X-ray

$I_0$ ...intensity of the incident X-ray

$\frac{\mu}{\rho}$ ...mass attenuation coefficient

$\rho$ ...density

$d$ ...thickness

According to equation 2.1, the higher  $\mu/\rho$  and the thicker the sample is, the more absorption takes place and, thus, the less intensity of the transmitted X-rays will be measured. Each element has tabulated values for MACs at different photon energies. The physical effects underlying the Beer-Lambert law within energies below 1 MeV are the photoelectric effect, elastic (Thomson) scattering and inelastic (Compton) scattering. Calculated MAC's rely heavily on theoretical values of the total cross section per atom  $\sigma_{tot}$  related to  $\frac{\mu}{\rho}$  according to [4]

$$\frac{\mu}{\rho} = \sigma_{tot} \left( \frac{N_A}{A_r} \right) \quad (2.2)$$

$N_A$ ...Avogadro's number

$A_r$ ...relative atomic mass

$\sigma_{tot}$  can be written as the sum over contributions from the principal photon interactions.

$$\sigma_{tot} = \sigma_{coh} + \sigma_{incoh} + \tau + \kappa + \sigma_{ph.n.} \quad (2.3)$$

$\sigma_{coh}$ ...coherent (Rayleigh) scattering cross section

$\sigma_{incoh}$ ...incoherent (Compton) scattering cross section

$\tau$ ...atomic photo-effect cross section

$\kappa$ ...positron-electron pair-production cross section

$\sigma_{ph.n.}$ ...photo-nuclear cross section

The value of  $\mu/\rho$  for a particular X-ray within a specimen is calculated by the sum over the mass absorption coefficients for each element times their weight fraction [2]. The absorption of the specific X-ray line originating from element A by all elements  $i$  is summarized including the self-absorption by element A.

$$\left[ \frac{\mu}{\rho} \right]_{spec}^A = \sum_i C_i \left[ \frac{\mu}{\rho} \right]_i^A \quad (2.4)$$

where  $C_i$  is the fractional concentration of element  $i$  in the specimen such that

$$\sum_i C_i = 1 \quad (2.5)$$

## 2.3 Quantitative X-ray analysis

In EDXS, it is easy to qualitatively analyze a material by assigning the peaks of an EDX spectrum to their corresponding elements. But when it comes to the elemental concentration of the observed area, one has to apply a quantitative analysis. To apply quantification methods, it is necessary to determine not only the locations of the peaks at the energy scale, but also their intensities. The peak intensity is equal to the area underneath the peak and is calculated by integration. As mentioned above, the spectrum contains characteristic peaks and bremsstrahlung which has to be subtracted to get the net intensities of the X-ray lines. The resulting intensities are the basis for each quantification method to finally calculate concentrations.

### 2.3.1 The Cliff-Lorimer method

Cliff and Lorimer (1975) suggested a method for determining relative concentrations by measuring the ratio of two element-specific intensities  $\left( \frac{I^A}{I^B} \right)$  [1]. This ratio is proportional

to the ratio of concentrations.

$$\frac{c_A}{c_B} = k_{AB} \frac{I_A}{I_B} \quad (2.6)$$

$c_A, c_B$ ...concentrations in weight percent of element A resp. B  
 $I_A, I_B$ ...intensities of the corresponding X-ray lines above background  
 $k_{AB}$ ...proportionality factor

The proportionality factor  $k_{AB}$  is called the Cliff-Lorimer factor or k-factor and, if it is known, the concentrations can be determined by measuring intensities under the assumption that  $\sum_i C_i = 1$ . The k-factor varies depending on the high-voltage of the microscope and the detector but is not dependent on the thickness and the composition of the specimen. If the so-called thin film criterion (TFC) is fulfilled, absorption within the specimen can be ignored. Since fluorescence is usually a minor effect it is neglected [2]. The thinner the observed area is, the less absorption/fluorescence will occur (see chapter 2.2).

k-factors can be determined by calculations from first principles or experimentally. Both approaches have crucial drawbacks. The experimental determination is time-consuming and needs well defined standards. The relative error is about 1%. Although the theoretical calculations are fast, the precision decreases substantially, leading to relative errors of about 15 – 20% [5].

The main limitation of the Cliff-Lorimer method is that an absorption correction is only possible if the mass thickness is known which is usually not the case for an unknown specimen (Horita et al. [6]). For low-energy X-ray lines, the TFC is no longer valid because these lines are absorbed to a high extent even in very thin specimens. This fact makes a proper absorption correction essential to get reliable results for light elements.

### 2.3.2 The $\zeta$ -factor method

If we consider that the TFC is valid in a TEM sample, the measured intensity is proportional to the mass thickness and the corresponding elemental concentration. The proportionality factor which connects this relation is called  $\zeta$ -factor [1]. To make this factor independent of the beam current and the acquisition time of the spectrum, it is normalized by the total electron dose.

The  $\zeta$ -factor method has several advantages compared to the Cliff-Lorimer method, especially a much easier application of an absorption correction.

$$\rho t = \zeta_A \frac{I_A}{c_A D_e} \quad (2.7)$$

with

$$D_e = N_e I_p \tau \quad (2.8)$$

$t$ ...thickness

$\rho$ ...density

$\rho t$ ...mass thickness

$I_A$ ...intensity of the characteristic X-ray line of element A

$c_A$ ...mass fraction of element A

$D_e$ ...total electron dose

$N_e$ ...number of electrons in one unit of electric charge

$\tau$ ...acquisition time

Therefore,  $\zeta$ -factors are element-specific quantities. To be more precise, each characteristic X-ray line family of each element has its own  $\zeta$ -factor. As mentioned above, the  $\zeta$ -factor is not dependent on current, concentration, composition and mass thickness by definition. It summarizes all attributes of generation and detection of X-rays within a specific instrument, including detector and collection efficiency. This means that each microscope has different  $\zeta$ -factors as every system has different detectors/detector arrangements. Basically,  $\zeta$ -factors can be determined either theoretically or experimentally. The intensity of characteristic X-rays originating from element A is theoretically described by [7]

$$I_A = N \frac{Q_A \omega_A a_A}{M_A} c_A \rho t D_e \left( \frac{\Omega}{4\pi} \right) \epsilon_A \quad (2.9)$$

$N$ ...Avogadro's number

$Q_A$ ...ionization cross section

$\omega_A$ ...fluorescence yield

$a_A$ ...relative line intensity ratio

$M_A$ ...atomic weight

$\Omega/(4\pi)$ ...detector solid angle

$\epsilon_A$ ...detector efficiency

If we compare equation 2.7 and 2.9, the  $\zeta$ -factor can be expressed as:

$$\zeta_A = \frac{M_A}{N Q_A \omega_A a_A \left( \frac{\Omega}{4\pi} \right) \epsilon_A} \quad (2.10)$$

If all these parameters are known, it is possible to calculate  $\zeta$ -factors. Nevertheless, it is very hard to get accurate values, especially for  $Q_A$ ,  $\omega_A$  and  $a_A$ . Thus, the experimental approach is often preferred. There are several methods for determining  $\zeta$ -factors experimen-

tally. The limiting factor for accuracy is generally the thickness measurement. Kothleitner et al. [8] prepared a lamella and a needle of the same material by means of a focused ion beam. The needle with a well defined shape was used to obtain the inelastic mean free path  $\lambda$  which was then applied to measure the thickness of the lamella (see section 2.4.4). Since it is not possible to get rid of amorphous layers during the needle preparation, the value for  $\lambda$  is error-prone. The advantage of this technique is that it can be applied to all kinds of materials.

Watanabe et al. [1] used a glass standard (NIST SRM2063a) with known thickness and composition. From this standard,  $\zeta$ -factors for all incorporated elements can be determined directly. To gain  $\zeta$ -factors for other elements, one has to apply a mathematical fit using models for the above mentioned parameters (like ionization cross section ...) . The need for this particular standard as well as uncertainties related to the fitting procedure are major drawbacks of this strategy.

In a third approach developed by Zanaga et al. [9], nanoparticles with a known geometry (determined by electron tomography) of the specimen were used. Due to the complexity of this measuring procedure and the fact that it is restricted to specific materials, this method is not universally applicable. Therefore, the need for a new approach which can be applied to a wide range of materials and does not require thickness measurement is evident.

Once reliable  $\zeta$ -factors are obtained for your system, they can be used for quantification. Equation 2.7 is valid for each compound of the system, and, if reformulated, it is possible to express mass thickness and concentrations as follows:

$$\rho t = \frac{\zeta_A I_A + \zeta_B I_B}{D_e}, \quad c_A = \frac{\zeta_A I_A}{\zeta_A I_A + \zeta_B I_B}, \quad c_B = \frac{\zeta_B I_B}{\zeta_A I_A + \zeta_B I_B} \quad (2.11)$$

For equation 2.11, a binary system with the elements A and B is assumed. However, this approach can be expanded to any multi-component specimen. Hence, it is possible to attain the concentrations as well as the mass thickness of the analyzed region just by measuring X-ray intensities and the beam current.

#### Absorption correction for the $\zeta$ -factor method

As mentioned above, the concept explained in chapter 2.3.2 is only valid if the TFC is fulfilled, meaning that X-ray absorption within the specimen can be neglected. However, if this is not the case, an X-ray absorption correction has to be applied. This is done with an iterative procedure which is described by Watanabe et al. [1]. After the calculation of the initial mass thickness and compositions, the different correction terms are determined and added to the equations 2.11 in the way it is shown in figure 2.3. Once the corrected values are calculated they are either used to calculate new, more proper correction terms or are considered as final concentration and mass thickness if there is no more change.

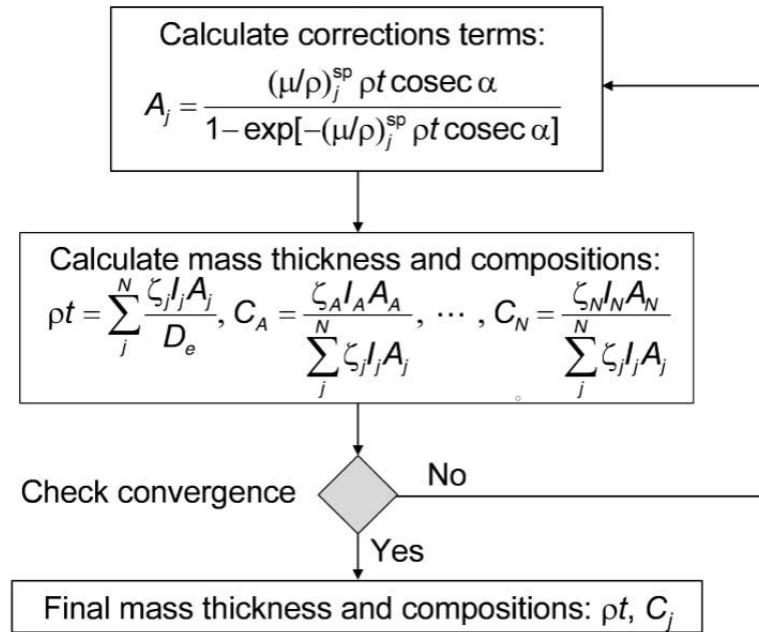


**Figure 2.3:** A flow chart of the quantification procedure in the  $\zeta$ -factor method with the X-ray absorption correction. (taken from Watanabe et al. [1])

The absorption correction term depends on the MAC of the corresponding X-ray line in the specimen, the take-off angle  $\alpha_{TO}$  and the mass thickness (see equation 2.12) [10]. Since the mass thickness is a result of the  $\zeta$ -factor method itself, the effort to apply an absorption correction is much lower compared to the Cliff-Lorimer method.

$$A_A = \frac{\left[ \frac{\mu}{\rho} \right]_{spec}^A \rho t \operatorname{cosec} \alpha_{TO}}{1 - \exp \left[ - \left[ \frac{\mu}{\rho} \right]_{spec}^A \rho t \operatorname{cosec} \alpha_{TO} \right]} \quad (2.12)$$

$A_A$ ...absorption correction term

Equation 2.12 is valid for a parallel slab geometry of the specimen.

The X-ray take-off angle  $\alpha_{TO}$  is used to calculate the distance which an X-ray has to travel through before it is detected. This distance is called the absorption path length and influences the absorption in accordance to equation 2.12.

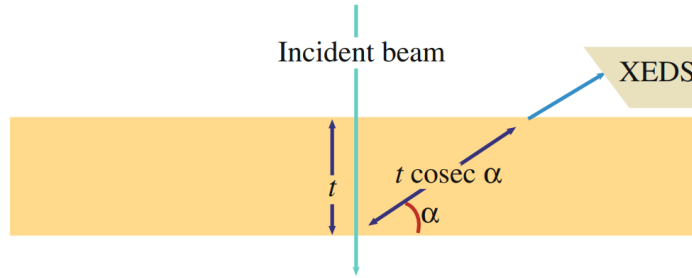


**Figure 2.4:** Relationship between the specimen thickness  $t$  and the absorption path length  $t \cdot \text{cosec } \alpha_{TO}$ , for a take-off angle  $\alpha_{TO}$ . (taken from D. B. Williams et al. [2])

The take-off angle  $\alpha_{TO}$  is determined by the geometry of the EDX system (detector elevation angle) and the specimen tilt which can be adjusted by the TEM's operator. If a double tilt specimen holder is used, it is possible to tilt the specimen in two directions, namely into the  $\alpha$  and  $\beta$  direction. The take-off angle depends on the alpha and beta tilt as follows [11]:

$$\sin \alpha_{TO} = \frac{\cos \vartheta_e (\sin \beta \cos \vartheta_a - \sin \alpha \cos \beta \sin \vartheta_A) + \cos \alpha \cos \beta \sin \vartheta_e}{\sqrt{(\sin \beta \cos \vartheta_a - \sin \alpha \cos \beta \sin \vartheta_A)^2 + (\cos \alpha \cos \beta)^2}} \quad (2.13)$$

$\vartheta_e$ ...detector elevation angle

$\vartheta_A$ ...detector azimuthal angle

## 2.4 Extrapolation methods - new approaches for $\zeta$ -factor determination

In order to measure correct k-factors or  $\zeta$ -factors for light elements, it is necessary to take absorption into account. It is mandatory to know the mass thickness of the specimen to calculate the absorption correction term (equation 2.12). Though, thickness determination can be tedious and inaccurate. The two main possibilities for measuring the specimen thickness in a TEM is via the  $\frac{t}{\lambda}$ -method or via CBED measurements [12], [13]. The first one yields a value which is relative to the inelastic mean free path  $\lambda$  of the incident electron in the specimen. Only if  $\lambda$  is known, an absolute value for the thickness can be calculated. However, theoretical and experimental methods for the  $\lambda$ -determination are error-prone. The second method using CBED is only applicable for crystalline parts of the specimen and disregard all amorphous layers. Hence, both methods are not satisfying.

### 2.4.1 Horita plots

Horita et. al. [14] have developed an extrapolation method for determining the absorption free k-factor to overcome this issue. Generally, the k-factor can be connected to the

element-specific  $\zeta$ -factors by

$$k_{AB} = \frac{\zeta_A}{\zeta_B} \quad (2.14)$$

if we compare equation 2.6 and 2.7.

The idea of the extrapolation method by Horita et al. [14] is to measure X-ray spectra at different specimen thicknesses. The intensity of an X-ray line is considered as a measure for thickness. If this X-ray line is not absorbed its intensity is proportional to the film thickness. Based on the measurements at different thicknesses an extrapolation to zero thickness is made to obtain an absorption free k-factor.

In a Horita plot the k-factor is plotted against a non-absorbed X-ray line intensity and could be misunderstood as a thickness dependent parameter which is not the case if we consider equation 2.6. In fact, the k-factor is a relation of a concentration ratio and an intensity ratio. The intensity ratio is thickness dependent if absorption takes place.

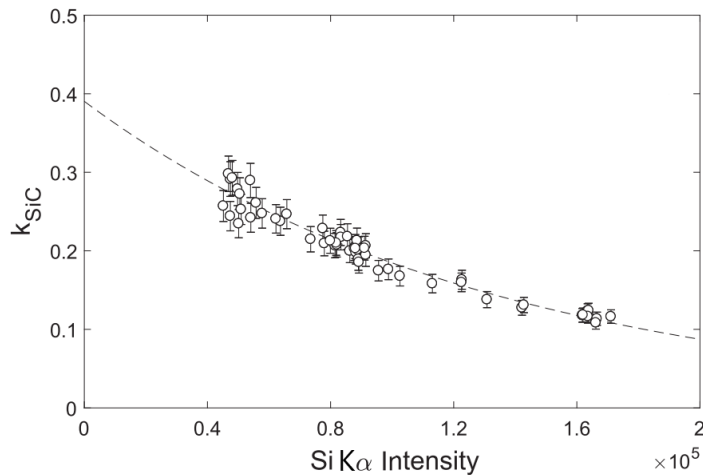


**Figure 2.5:** Example of a Horita plot showing measuring points at different thicknesses. The thickness is represented by the silicon  $K\alpha$ -line intensity of a SiC crystal. The intersection of the exponential fit with the ordinate indicates the absorption-free k-factor. (taken from Marvel et al. [15])

Regarding equation 2.14, this means that  $\zeta_A$  can be calculated, if  $\zeta_B$  is known, and vice versa. This fact can be used in particular to determine  $\zeta$ -factors of light elements, which are very often part of chemical compounds, if the  $\zeta$ -factor of the second element is already known.

Marvel et al. [15] use a standard glass thin film (NIST SRM2063a) with a known composition and thickness to directly measure the  $\zeta$ -factor of the silicon K-line. Afterwards, they measured Horita plots to get the absorption-free k-factors of SiC and SiB<sub>6</sub>. For each



series of measurements the silicon  $K\alpha$  intensity represents the thickness (see figure 2.5). Since the  $\zeta$ -factor of the silicon K-line is already known, the  $\zeta$ -factors for carbon and boron are calculated according to equation 2.14.

We were inspired by the work of Marvel et al. [15] and advanced their method to determine  $\zeta$ -factors especially for light elements by using the fitting parameters of such Horita plots. Since the shape of the curve represents the magnitude of absorption, it should be possible to give the fitting parameters a physical meaning and, if all other parameters are known, to calculate  $\zeta$ -factors from them without measuring the specimen thickness. The following three chapters will explain the derivation of  $\zeta$ -factors using the absorption of X-ray lines within the specimen. In every explanation, a binary system in which A and B are different elements is considered. Furthermore, each approach results in a modified Horita plot where the abscissa represents a measure for thickness and the ordinate an X-ray intensity or a ratio of intensities.

#### 2.4.2 Method **A** - Thickness dependence of $k_{AB}$ -factor

In this first ansatz, the resulting dependence reflects a classic Horita plot. The starting points are the equations 2.6, 2.9, 2.12 and 2.14. Under the assumption that the X-rays of element B are not absorbed ( $A_B = 1$ ) and are therefore a valid measure for thickness, we can write the line intensities of A and B

$$I_A = c_A \frac{N\rho t}{M_A} D_e(Q\omega a)_A \frac{1}{A_A} \left( \frac{\Omega}{4\pi} \epsilon_A \right) \quad (2.15)$$

$$I_B = c_B \frac{N\rho t}{M_B} D_e(Q\omega a)_B \left( \frac{\Omega}{4\pi} \epsilon_B \right) \quad (2.16)$$

If we put these intensities into equation 2.6, we get

$$k_{AB} = \frac{M_A(Q\omega a)_B \epsilon_B}{M_B(Q\omega a)_A \epsilon_A} A_A = \frac{M_A(Q\omega a)_B \epsilon_B}{M_B(Q\omega a)_A \epsilon_A} \frac{(\rho t) \operatorname{cosec} \alpha_{TO} \sum_i c_i \frac{\mu}{\rho} \Big|_i^A}{1 - e^{-(\rho t) \operatorname{cosec} \alpha_{TO} \sum_i c_i \frac{\mu}{\rho} \Big|_i^A}} \quad (2.17)$$

which is a function of t. If we reformulate equation 2.16 and substitute t in 2.17 with the non-absorbed intensity  $I_B$ , we get the following dependence:

$$k_{AB} = I_B \frac{\frac{M_A \sum_i c_i \frac{\mu}{\rho} \Big|_i^A}{c_B N(Q\omega a)_A \epsilon_A D_e \left( \frac{\Omega}{4\pi} \right) \sin \alpha_{TO}}}{1 - e^{-\frac{I_B M_B \sum_i c_i \frac{\mu}{\rho} \Big|_i^A}{c_B N(Q\omega a)_B D_e \left( \frac{\Omega}{4\pi} \epsilon_B \right) \sin \alpha_{TO}}} \quad (2.18)$$

which is of the form

$$y = \frac{g_1 x}{1 - e^{-g_2 x}} \quad \text{with} \quad y = k_{AB}, \quad x = I_B \quad (2.19)$$

$g_1, g_2$ ...fitting parameters of the Horita plot

and

$$g_1 = \frac{\sum_i c_i \frac{\mu}{\rho}]_i^A}{c_B D_e \sin \alpha_{TO}} \frac{M_A}{N(Q\omega a)_A \left(\frac{\Omega}{4\pi}\right) \epsilon_A} \quad (2.20)$$

$$g_2 = \frac{\sum_i c_i \frac{\mu}{\rho}]_i^A}{c_B D_e \sin \alpha_{TO}} \frac{M_B}{N(Q\omega a)_B \left(\frac{\Omega}{4\pi}\right) \epsilon_B} \quad (2.21)$$

By comparing equation 2.20 and 2.21 with equation 2.10, the  $\zeta$ -factors for both elements can be calculated by

$$\zeta_A = \frac{g_1 c_B D_e \sin \alpha_{TO}}{\sum_i c_i \frac{\mu}{\rho}]_i^A} \quad (2.22)$$

$$\zeta_B = \frac{g_2 c_B D_e \sin \alpha_{TO}}{\sum_i c_i \frac{\mu}{\rho}]_i^A} \quad (2.23)$$

The  $\zeta$ -factors for both elements are calculated from the fitting parameters of the Horita plot and the other known quantities (concentrations, MAC, take-off angle and electron dose).

### 2.4.3 Method **B** - Intensity dependence of reference intensity

The second ansatz stems from a slightly modified version of the Horita plot where the  $k$ -factor no longer represents the ordinate but the intensity of the X-ray line which experiences absorption. The abscissa is still represented by the intensity of the non-absorbed ( $A_B = 1$ ) X-ray line. If we merge equation 2.15 with equation 2.10 and 2.12, we get the following for

the absorbed X-ray line:

$$I_A = \frac{D_e c_A \sin \alpha_{TO} \left[ 1 - e^{-\frac{\rho t \sum_i c_i \frac{\mu}{\rho}]_i^A}{\sin \alpha_{TO}}} \right]}{\zeta_A \sum_i c_i \frac{\mu}{\rho}]_i^A} \quad (2.24)$$

If equation 2.7 is altered by putting  $t$  on the left side alone and substitute  $t$  in equation 2.24 with it, one gets

$$I_A = \frac{D_e c_A \sin \alpha_{TO}}{\zeta_A \sum_i c_i \frac{\mu}{\rho}]_i^A} \left[ 1 - e^{-\frac{\zeta_B I_B \sum_i c_i \frac{\mu}{\rho}]_i^A}{D_e c_B \sin \alpha_{TO}}} \right] \quad (2.25)$$

which is of the form:

$$y = h_1 \left[ 1 - e^{-x h_2} \right] \quad \text{with} \quad y = I_A, \quad x = I_B \quad (2.26)$$

$h_1, h_2$ ...fitting parameters of the modified Horita plot

and

$$h_1 = \frac{D_e \sin \alpha_{TO} c_A}{\sum_i c_i \frac{\mu}{\rho}]_i^A \zeta_A} \quad (2.27)$$

$$h_2 = \frac{\sum_i c_i \frac{\mu}{\rho}]_i^A \zeta_B}{D_e \sin \alpha_{TO} c_B} \quad (2.28)$$

Again, the  $\zeta$ -factors  $\zeta_A$  and  $\zeta_B$  can be calculated by the fitting parameters and reformulating equation 2.27 and 2.28.

Method B is very similar to method A, since the same information is used to perform both fits. The only difference is that the quasi non-absorbed X-ray line is used twice in method A - within the k-factor and as a measure for thickness.

#### 2.4.4 Method C - Intensity dependence of $\frac{t}{\lambda}$

In the third derivation used to determine  $\zeta$ -factors from fitting parameters, the measure for thickness is changed from a non-absorbing X-ray line intensity to the relative thickness

which is measured by EELS and is defined as

$$\frac{t}{\lambda} = \ln \left( \frac{I_{tot}}{I_0} \right) \quad (2.29)$$

$t$ ...specimen thickness

$\lambda$ ...inelastic mean free path

$I_{tot}$ ...intensity of the whole spectrum

$I_0$ ...intensity of the zero loss peak

If the inelastic mean free path of the material is known, it is possible to obtain the absolute thickness by rewriting formula 2.29 as:

$$t = \lambda \cdot \ln \left( \frac{I_{tot}}{I_0} \right) \quad (2.30)$$

The derivation starts again with the relation for the X-ray line of element A which suffers from absorption (see equation 2.15). Here, equation 2.10 is inserted and the  $\zeta$ -factor is brought to the left side.

$$\zeta_A = \frac{\rho t c_A D_e}{I_A} \frac{1}{A_A} \quad (2.31)$$

The absorption correction term (equation 2.12) is inserted and each thickness-term is divided and multiplied by  $\lambda$ , which gives

$$\zeta_A = \frac{\frac{t}{\lambda} \lambda \rho c_A D_e}{I_A} \frac{1 - e^{-\frac{t}{\lambda} \lambda \rho \text{cosec} \alpha_{TO} \sum_i c_i \frac{\mu}{\rho}}_i^A}{\frac{t}{\lambda} \lambda \rho \text{cosec} \alpha_{TO} \sum_i c_i \frac{\mu}{\rho}}_i^A} \quad (2.32)$$

The above-mentioned formula can be rewritten as

$$I_A = \frac{c_A D_e \sin \alpha_{TO}}{\zeta_A \sum_i c_i \frac{\mu}{\rho}}_i^A} \frac{1 - e^{-\frac{t}{\lambda} \lambda \rho \text{cosec} \alpha_{TO} \sum_i c_i \frac{\mu}{\rho}}_i^A}}{1} \quad (2.33)$$

which is of the form

$$y = f_1 \left[ 1 - e^{-x f_2} \right] \quad \text{with} \quad y = I_A, \quad x = \frac{t}{\lambda} \quad (2.34)$$

$f_1, f_2$ ...fitting parameters of the modified Horita plot

and

$$f_1 = \frac{c_A D_e \sin \alpha_{TO}}{\zeta_A \sum_i c_i \left[ \frac{\mu}{\rho} \right]_i^A} \quad (2.35)$$

$$f_2 = \lambda \rho \operatorname{cosec} \alpha_{TO} \sum_i c_i \left[ \frac{\mu}{\rho} \right]_i^A \quad (2.36)$$

$\zeta_A$  and  $\lambda$  can be calculated by rewriting the equations 2.35 and 2.36.  $\zeta_B$  is determined according to equation 2.14. Therefore, it is necessary to perform an additional Horita plot to obtain the absorption-free k-factor like it is explained in chapter 2.4.1. Since we want to avoid to use the assumption of a non-absorbed X-ray line the measure for thickness is represented by the relative thickness  $\frac{t}{\lambda}$  in this version of a Horita plot. The advantage of this method is that one can not only determine both  $\zeta$ -factors but also the specimen's inelastic mean free path if the density is known. Moreover, the assumption of a non-absorbing X-ray line is no longer necessary.



# CHAPTER 3

---

## Experiments and results

---

Elemental standards are needed to put the procedures, described in the theoretical part, into practice. These standards have to be prepared in a way that the resulting specimen has regions with different thicknesses, at which, EDXS measurements are taken. For each method a current measurement is required. Method C, additionally needs an EELS measurement at each region where an EDX spectrum is acquired. An evaluation routine needs to be implemented for both, the EDX spectra and the created fits.

EDXS and EELS spectrum images (to increase the measurement efficiency), were acquired simultaneously at different thicknesses on each crystalline specimen. Every single spectrum was evaluated with respect to X-ray intensities (EDXS) and  $\frac{t}{\lambda}$ -values. The data was then used to acquire Horita plots, perform exponential fits and determine the  $\zeta$ -factors from the fitting parameters.

### 3.1 Specimens

#### 3.1.1 Choice of samples

For the determination of  $\zeta$ -factors via extrapolation and fitting methods, both, the composition of the specimen and its thickness distribution, are vital to get reliable results. Since these methods depend on the effect of X-ray absorption, it is necessary to ensure that enough absorption takes place within the specimen. As described in chapter 2.2 the probability for low-energy X-rays of light elements to be absorbed is much higher than for high-energy X-rays which originate from heavier elements. Another criterion for the choice of the sample is that it emits one X-ray line which hardly suffers from absorption. This non-absorbing line can be used as a measure for thickness. The standard has to have constant composition and density, hence, it is feasible to work with single crystals. Furthermore, the energies of the generated X-ray lines should be well separated. This simplifies the evaluation of the EDX-spectra. Moreover, the sample should be stable under the electron beam, thinned to electron transparency and should not contain elements used in microscope components or elements which can be implanted during specimen preparation.

Since the method is based on EDXS/EELS measurements at different thicknesses, it is obvious that the sample needs to have a proper thickness distribution which can be achieved by a wedge-shaped lamella.

In this work, single crystals of three materials were chosen. Their densities and compositions are listed in table 3.1

**Table 3.1:** Materials used for the acquisition of EDXS and EELS spectrum images  
*c*...concentration in percentage by mass [wt%]  
*ρ*...density [g/cm<sup>3</sup>]

Silicon dioxide single crystal (Quartz crystal)	SiO <sub>2</sub> <i>c</i> <sub>Si</sub> = 46.74 wt%, <i>c</i> <sub>O</sub> = 53.26 wt% <i>ρ</i> = 2.65 g/cm <sup>3</sup>
Zinc oxide single crystal	ZnO <i>c</i> <sub>Zn</sub> = 80.34 wt%, <i>c</i> <sub>O</sub> = 19.65 wt% <i>ρ</i> = 5.61 g/cm <sup>3</sup>
Silicon carbide 4H single crystal	SiC <i>c</i> <sub>Si</sub> = 70.04 wt%, <i>c</i> <sub>C</sub> = 29.96 wt% <i>ρ</i> = 3.21 g/cm <sup>3</sup>

The values for the mass attenuation coefficients in table 3.2 were calculated with equation 2.4. The values of the individual elements' MACs were taken from the website of the National Institute of Standards and Technology (NIST) [16]. The lower the atomic number *Z* of the ionized atom within the specimen, the higher the value of the MAC for the emitted X-ray lines. Therefore, it is evident that low-energy X-rays get absorbed to a higher extent than X-rays with higher energies.

**Table 3.2:** MACs for Si and O in SiO<sub>2</sub>, Zn and O in ZnO, Si and C in SiC,  
 values taken for the K(*α*) lines,  
 source: NIST-database [16]

<b>SiO<sub>2</sub></b>	<i>ρ</i> <sub>SiO<sub>2</sub></sub> [g/cm <sup>3</sup> ]	<i>c</i> <sub>Si</sub> [wt%]	<i>c</i> <sub>O</sub> [wt%]	$\left[\frac{\mu}{\rho}\right]_{spec}^{Si}$ [m <sup>2</sup> /kg]	$\left[\frac{\mu}{\rho}\right]_{spec}^O$ [m <sup>2</sup> /kg]
	2.65	46.74	53.26	66.89	412.29
<b>ZnO</b>	<i>ρ</i> <sub>ZnO</sub> [g/cm <sup>3</sup> ]	<i>c</i> <sub>Zn</sub> [wt%]	<i>c</i> <sub>O</sub> [wt%]	$\left[\frac{\mu}{\rho}\right]_{spec}^{Zn}$ [m <sup>2</sup> /kg]	$\left[\frac{\mu}{\rho}\right]_{spec}^O$ [m <sup>2</sup> /kg]
	5.61	80.34	19.66	3.89	484.89
<b>SiC</b>	<i>ρ</i> <sub>SiC</sub> [g/cm <sup>3</sup> ]	<i>c</i> <sub>Si</sub> [wt%]	<i>c</i> <sub>C</sub> [wt%]	$\left[\frac{\mu}{\rho}\right]_{spec}^{Si}$ [m <sup>2</sup> /kg]	$\left[\frac{\mu}{\rho}\right]_{spec}^C$ [m <sup>2</sup> /kg]
	3.21	70.05	29.95	35.25	2462.60



### 3.1.2 Specimen preparation

The specimens were prepared from bulk material by means of a focused ion beam (FIB) with the FEI Nova 200 Nanolab. Every specimen was thinned to a wedge-shaped lamella and mounted on an Omniprobe grid. The goal of the preparation was to obtain a wedge angle in the range of 1-2° with different thicknesses. To avoid shadowing effects, the specimen was mounted on the grid in the so-called "top-position" (see figure 3.1).

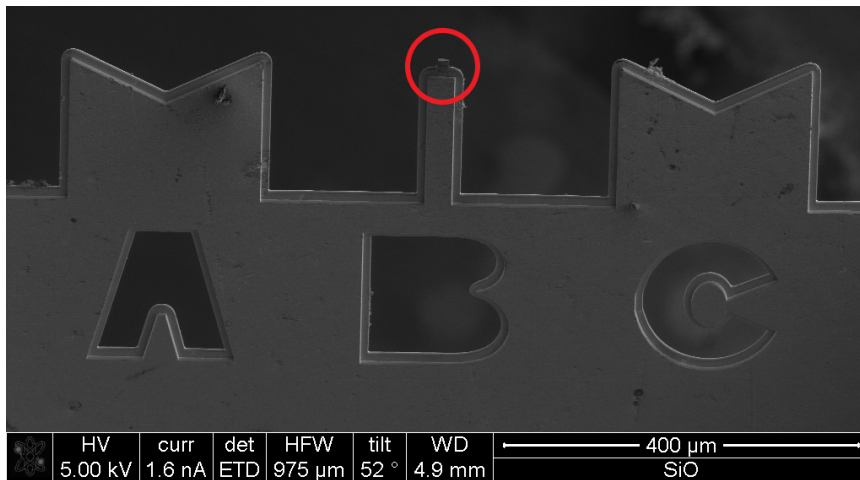


**Figure 3.1:** SiO<sub>2</sub> lamella mounted on an Omniprobe grid in top-position, SE image taken during FIB preparation

## 3.2 Used TEM-EDXS system

### FEI Titan (S)TEM

The Titan 60-300 is equipped with a high-brightness Schottky X-FEG with a monochromator. The operating voltage was 300 kV. A Cs-probe corrector for high-resolution STEM imaging, several HAADF, BF and ADF detectors and a high-resolution GIF (Gatan Imaging Filter) Quantum electron spectrometer for EELS and EFTEM are implemented. The Titan is provided with an EDXS detector system which is called Super-X detector. It contains four windowless SDD detectors placed symmetrically around the optical axis.

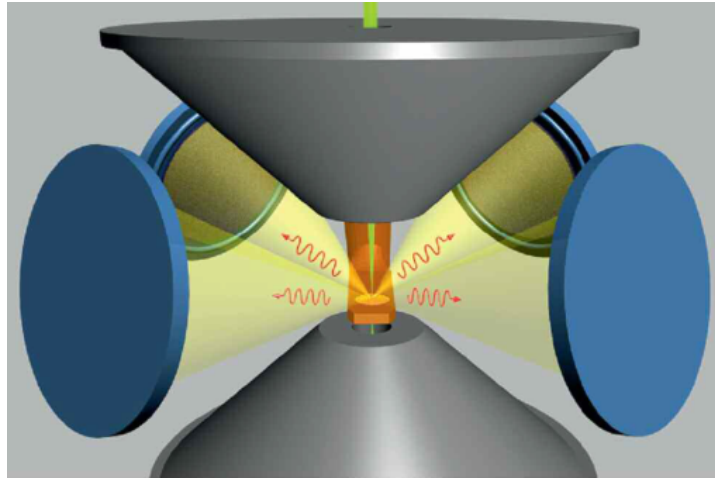


**Figure 3.2:** Schematic of the Super-X geometry: Four SDD detectors are arranged symmetrically around the sample (taken from Schlossmacher et al. [17]).

In addition to the top-position of the lamella on the grid, an analytical double tilt holder especially designed for the Super-X detector system was used for a further reduction of shadowing effects. To avoid channeling effects, the probe was tilted out of the zone axis towards the active quadrant of the detector. Since the four quadrants may differ slightly in terms of solid angle, only a single quadrant per measurement was turned on. These differences may also result in slightly different  $\zeta$ -factors which will be discussed later on.

#### Experimental set-up

The measurements were performed in STEM mode. The parameters for the acquisition of EDXS and EELS data are listed in table 3.3. A small camera length was selected to ensure that all electrons enter the GIF to get reliable current measurements via the drift tube. An acquisition time of 100 s was chosen to have good statistics in terms of X-ray counts. The specimen tilt was different for each measurement, since zone axis avoidance had to be considered.

**Table 3.3:** Measurement parameters

C1 aperture [ $\mu\text{m}$ ]	2000
C2 aperture [ $\mu\text{m}$ ]	50
C3 aperture [ $\mu\text{m}$ ]	2000
Convergence angle [mrad]	19.6
EELS collection semi angle [mrad]	37.7
Camera length [mm]	29.5
Spectrometer entrance aperture [mm]	5
Dispersion EDXS [eV/channel]	5
Dispersion EELS [ev/channel]	0.25
Voltage [kV]	300

### 3.3 Acquisition of required data

As described in chapter 2.4, the data needed to experimentally obtain  $\zeta$ -factors depends on the extrapolation method that is used. For the methods A and B, it is sufficient to measure the X-ray intensities of the respective X-ray lines at different thicknesses. Method C additionally requires the relative thickness  $\frac{t}{\lambda}$ . Therefore, at each measured point both, an EDX spectrum and an EEL spectrum, were acquired. At the beginning and after every 9th acquisition, the current of the electron beam was measured to check whether the current was stable. The points were distributed over a range of specimen thicknesses. To get good statistics, 90 points for each measurement series were recorded. The zinc oxide lamella is shown in figure 3.3. The indicated points mark where the measurements were performed. They are distributed from thin at the top to thick at the bottom (corresponds to a relative thickness range of  $\frac{t}{\lambda} \approx 0.2 \dots 1.6$ ). The first and the 11th point are located off the lamella to control the beam current.

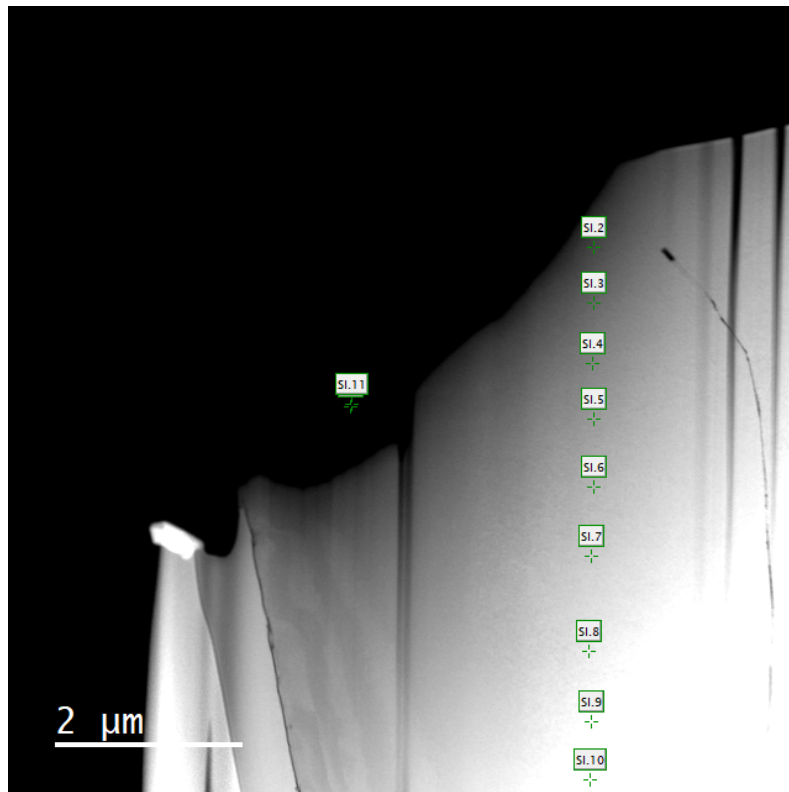
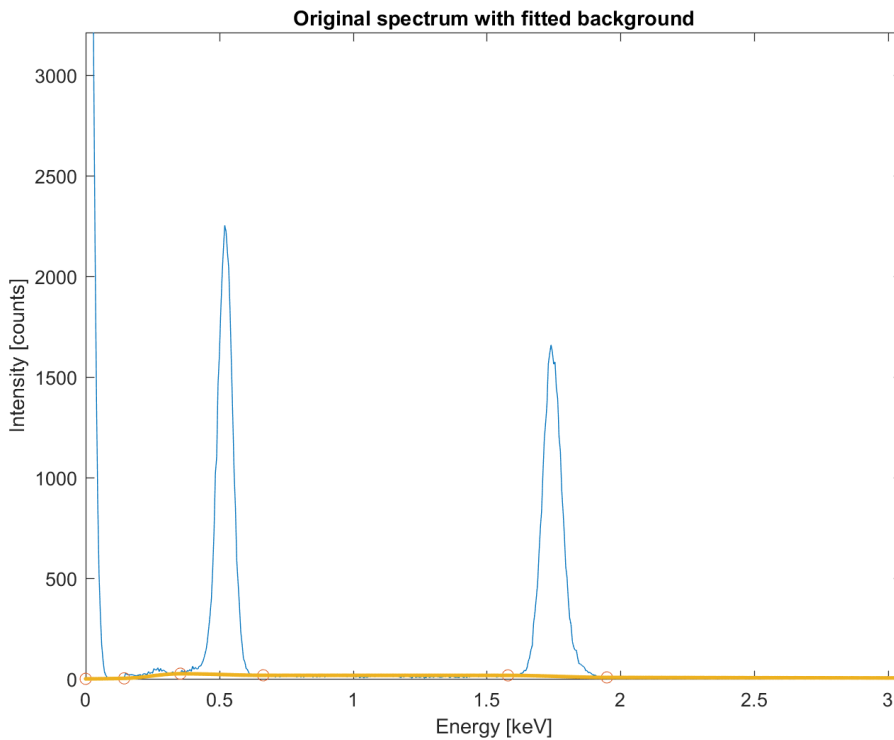


Figure 3.3: ZnO lamella with indicated measurement points

### 3.3.1 Determining peak intensities of EDX spectra

For the determination of the measured X-ray intensities, a Matlab script was written. Existing software was not used due to its unreliable background subtraction in the low-energy region. Moreover, only single spectra evaluation would have been possible which is very inefficient and time consuming. This script finds the desired peaks of the related X-ray lines, subtracts the background and evaluates the associated intensities. Figure 3.4 shows an example of an X-ray spectrum of  $\text{SiO}_2$ . The left peak represents the oxygen K-line, the right peak represents the silicon K-line. The background was fitted by the script with a polynomial function which was calculated from the orange-marked points in the figure. The position of the points at the edges of the peaks were read out manually from the software Digital Micrograph (DM) for each standard (see appendix for the whole script).



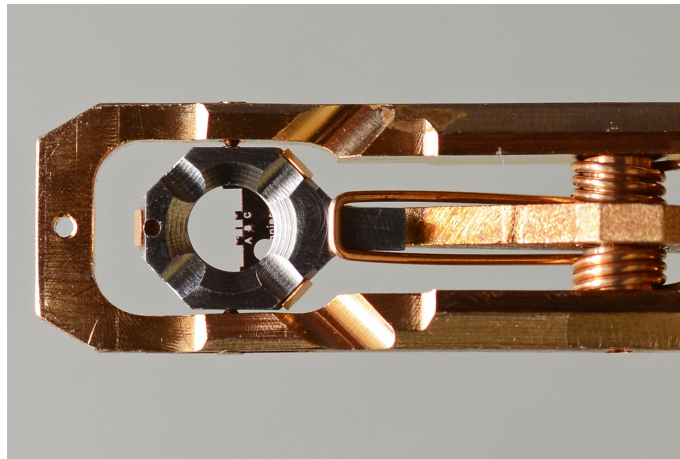
**Figure 3.4:** An original EDX spectrum of  $\text{SiO}_2$  with fitted background

### 3.3.2 Determination of $\frac{t}{\lambda}$ -values

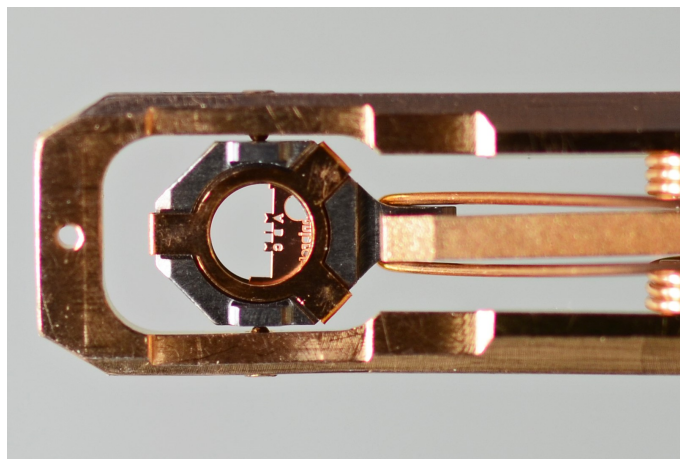
According to equation 2.29, the value of  $\frac{t}{\lambda}$  is obtained by calculating the natural logarithm of the fraction of the unfiltered EEL spectrum and the zero-loss filtered EEL spectrum. This is done automatically by DM. To get the absolute thickness  $t$ , the inelastic mean free path  $\lambda$  has to be known (see equation 2.30.)

### 3.4 $\zeta$ -factor determination

$\zeta$ -factors were measured for X-ray lines of the elements oxygen, carbon, silicon and zinc. Since oxygen and silicon are components of two used materials, two results were obtained and compared for these elements. The measurements were taken separately for detector I and detector II of the Super-X system. The relative orientation of the specimen to the EDX system in the microscope is an important factor to avoid shadowing effects. Therefore, the Omniprobe grid with the lamella was placed into the Super-X holder according to figure 3.5 for detector I and was rotated by 180° for detector II. Furthermore, the specimen was tilted towards the respective detector and out of zone axis to increase the efficiency and avoid channeling effects.



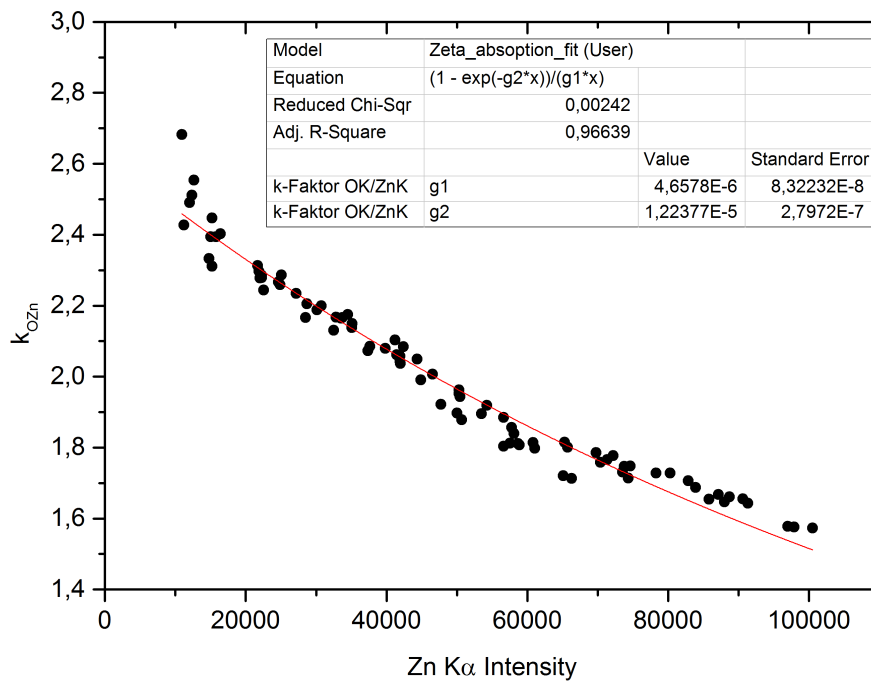
(a)



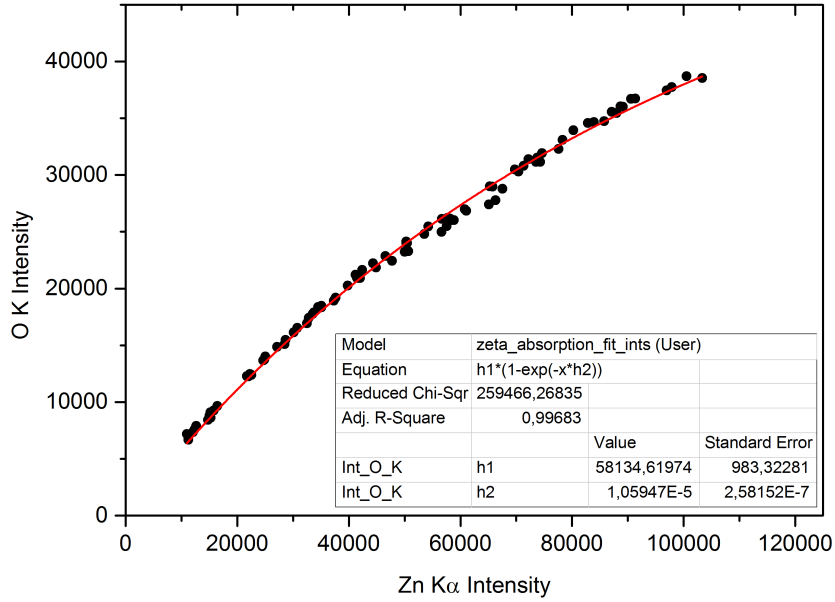
(b)

**Figure 3.5:** Orientation of the Omniprobe grid in the Super-X holder for detector I: (a) from top, (b) from below

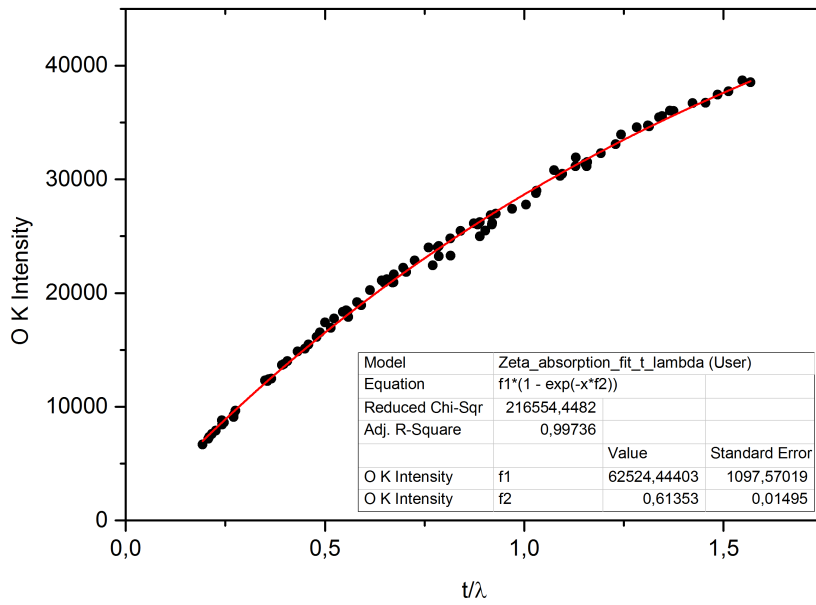
As described in chapter 2.4, four different kinds of graphs to determine  $\zeta$ -factors were generated. Either the ratio of the measured X-ray intensities (k-factor) or the line of the element which suffers from absorption, here the oxygen or carbon K-line, represents the ordinate. On the abscissa, a measure for thickness is plotted namely the X-ray intensity of the non-absorbed line or the  $\frac{t}{\lambda}$ -value. The graphs depict the effect of X-ray absorption in a descriptive way. The amount of X-rays increases with increasing thickness but at the same time more X-rays get absorbed, which is described by an exponential behavior (see figure 3.6). If an exponential fit whose equation is equal to either equation 2.19, 2.26 or 2.34 is applied, two fitting parameters are obtained in each case. Figure 3.6 shows all four graphs of ZnO at detector I. Figure 3.6 (a) is needed in order to perform method **A**, (b) for method **B** and (c) + (d) for method **C**. The implemented table within each graph depicts the calculated fitting parameters and their associated standard errors. All other graphs for ZnO, SiO<sub>2</sub> and SiC for both detectors can be found in the appendix.



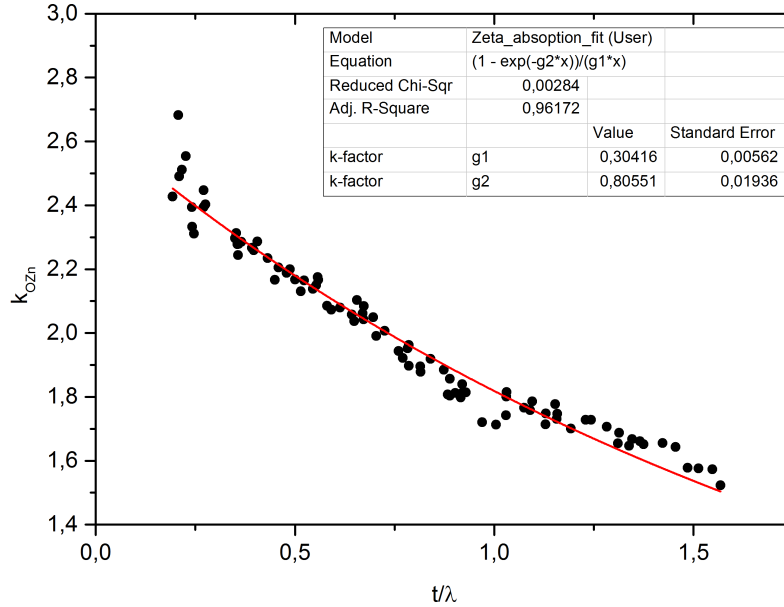
(a)



(b)



(c)



(d)

**Figure 3.6:** Graphs performed for  $\zeta$ -factor determination of ZnO at detector I; (a) k-factor dependence over Zn K $\alpha$  Intensity; (b) O K Intensity dependence over Zn K $\alpha$  Intensity; (c) O K Intensity dependence over  $\frac{t}{\lambda}$ ; (d) k-factor dependence over  $\frac{t}{\lambda}$

As discussed in chapter 2.2, the degree of absorption is determined by the MAC of a specific X-ray line within the specimen (see table 3.2). This means that the higher the MAC of a specific X-ray line, the larger the curvature of the exponential fit. In other words, the absorption in the specimen has to be sufficient in order to perform reliable fits. The data-points appear to lie close to the fitted lines, thus, the applied models (method A to C) are considered to work reasonably good. However, there seem to be differences in their quality.

#### Determination of the X-ray take-off angle $\alpha_{TO}$

To calculate  $\zeta$ -factors including X-ray absorption, the take-off angle  $\alpha_{TO}$  has to be known. The adjusted tilting angle of the specimen holder in combination with the geometry of the EDX system determines  $\alpha_{TO}$  (see equation 2.13). The azimuthal angle  $\vartheta_A$  is  $315^\circ$  for detector I and  $225^\circ$  for detector II. The elevation angle  $\vartheta_e$  is  $18^\circ$  (taken from Kraxner [11]). However, this is only the case if the lamella is considered to be mounted perfectly parallel to the Omniprobe grid. This was controlled by measuring the angle of the lamella within the FIB for all three specimens. The ZnO lamella was found to be slightly inclined in  $\beta$  direction with respect to the grid. At the other two lamellas (SiO<sub>2</sub> and SiC) no measurable inclinations have been noticed. This circumstance was considered by adding the measured divergence of  $1.4^\circ$  to the preset tilt angle  $\beta$  for measurements at the ZnO lamella.



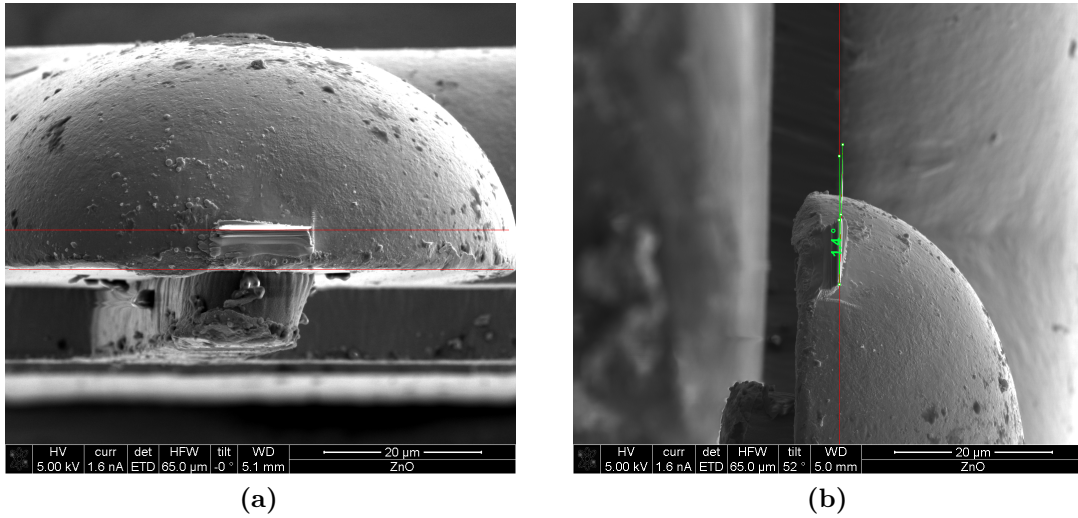


**Figure 3.7:** Angle measurement of the mounted ZnO lamella with respect to the Omniprobe grid: (a) shows the angle in  $\alpha$  direction ( $\alpha = 0^\circ$ ), (b) in  $\beta$  direction ( $\beta = 1.4^\circ$ ).

Although the mounting angle of the lamella was measured, a specific uncertainty for the X-ray take-off angle (estimated at  $0.5^\circ$ ) still has to be considered.

#### Determination of the electron dose $D_e$

According to equation 2.8, the electron dose is calculated from the beam current, the acquisition time and the elementary charge  $e$ . We noticed that the lifetime provided by DM was wrong since the numbers appeared to be higher than the chosen real time. Since the displayed dead time in the microscope's user interface was at 0% during the entire acquisition, we assume that the life time is very close to the real time. Therefore, the preset real time of 100 s was considered as the acquisition time and was used to calculate the electron dose. The beam current was measured frequently via the drift tube of the microscope's GIF before and after each measuring series. To assure that all electrons enter the drift tube when measuring without any specimen, a small camera length was chosen. The relative error of this measurement is considered to be 1%.

**Table 3.4:** Take-off angle and electron dose for each measured specimen at the detectors I and II

Specimen	Detector I		Detector II	
	$\alpha_{TO}$ [ $^\circ$ ]	$D_e$ [ $e^-$ ]	$\alpha_{TO}$ [ $^\circ$ ]	$D_e$ [ $e^-$ ]
<b>SiO<sub>2</sub></b>	$21.54 \pm 0.25$	$1.12 \cdot 10^{11}$	$24.39 \pm 0.25$	$1.13 \cdot 10^{11}$
<b>ZnO</b>	$36.71 \pm 0.25$	$1.07 \cdot 10^{11}$	$25.53 \pm 0.25$	$1.08 \cdot 10^{11}$
<b>SiC</b>	$27.27 \pm 0.25$	$1.08 \cdot 10^{11}$	$28.72 \pm 0.25$	$1.06 \cdot 10^{11}$

### 3.5 Results

For each specimen one data-set was acquired and evaluated with each of the two used detectors. Spectrum images (multipoint spectrum function of Digital Micrograph) were performed in order to increase the efficiency of the measurements. In the following three tables, the  $\zeta$ -factors of C-K, O-K, Si-K $\alpha$  and Zn-K $\alpha$  are listed. Each table represents the values obtained from one fitting method (**A**, **B** or **C**) according to equations 2.19, 2.26 and 2.34. Theoretically, each measured, element specific  $\zeta$ -factor should have the same value if it is measured with the same detector, no matter which method was used for evaluation. The  $\zeta$ -factors of O-K and Si-K $\alpha$  have been measured twice, since these elemental lines occur in more than one specimen. Errors were determined using single standard deviation (for the calculation see appendix C).

Table 3.5 displays  $\zeta$ -factors obtained from method **A**.

**Table 3.5:**  $\zeta$ -factors for K( $\alpha$ )-lines of C, O, Si and Zn determined from fitting parameters of the thickness dependent k-factor (method **A**) measured with the EDX detectors I and II. Errors were determined using single standard deviation.

Specimen	Element	$\zeta$ -factor $\left[ \frac{kg \cdot electron}{m^2 \cdot photon} \right]$	
		Detector I	Detector II
<b>SiO<sub>2</sub></b>	Si	472 ± 28	410 ± 20
	O	456 ± 24	395 ± 19
<b>ZnO</b>	Zn	1302 ± 50	1495 ± 64
	O	496 ± 17	542 ± 19
<b>SiC</b>	Si	553 ± 44	562 ± 37
	C	908 ± 43	912 ± 32

The weak point of this method is that it is based on the premise that the X-ray line of the heavier element is a valid measure for thickness, which is only true to a certain extent. Also, this X-ray energy could be absorbed which depends on the MAC of the respective X-ray line. For example, the MAC-value of the Si-K $\alpha$  line in SiO<sub>2</sub> is 66.89  $\frac{kg}{m^2}$ . Since the MAC of the O-K line in SiO<sub>2</sub> (412.29  $\frac{kg}{m^2}$ ) is only about six times higher this may lead to an substantial error. The situation for ZnO and SiC, with MAC-ratios of the associated X-ray lines of about 125 and 70, is different. Moreover, the MACs of the O-K line in ZnO (484.89  $\frac{kg}{m^2}$ ) and the C-K line in SiC (2462.60  $\frac{kg}{m^2}$ ) have larger absolute values than the O-K line in SiO<sub>2</sub>. This matter of fact gives rise to more absorption of the named X-ray lines within ZnO and SiC compared to SiO<sub>2</sub> and thus, more accurate fitting parameters and  $\zeta$ -factors.

None the less, the results for the  $\zeta$ -factors of all elements are already similar to the values that Fladischer and Kraxner achieved with other methods for the same system (see PhD thesis of Fladischer and Kraxner [18], [11]). Therefore, MAC-values of about 400  $\frac{kg}{m^2}$  for the

well absorbed X-ray line of the light element seem to be sufficient to perform exponential fits used in method **A**.

Since method **B** (table 3.6) uses the same kind of information to determine  $\zeta$ -factors the above mentioned arguments ought to be valid as well. The observable differences of the determined  $\zeta$ -factors could be explained by the usage of a different fitting function. Furthermore, the measured X-ray intensity of the quasi non-absorbed X-ray line no longer is used twice in order to calculate Cliff-Lorimer factors and as a measure for thickness. Hereby, some differences for the resulting  $\zeta$ -factors could emerge.

**Table 3.6:**  $\zeta$ -factors for K( $\alpha$ )-lines of C, O, Si and Zn determined by fitting parameters of the thickness-dependent intensity (method **B**) measured with the EDX detectors I and II. Errors were determined using single standard deviation.

Specimen	Element	$\zeta$ -factor $\left[ \frac{\text{kg-electron}}{\text{m}^2\text{-photon}} \right]$	
		Detector I	Detector II
<b>SiO<sub>2</sub></b>	Si	$519 \pm 27$	$443 \pm 20$
	O	$490 \pm 22$	$420 \pm 16$
<b>ZnO</b>	Zn	$1127 \pm 45$	$1422 \pm 61$
	O	$448 \pm 15$	$524 \pm 17$
<b>SiC</b>	Si	$498 \pm 43$	$554 \pm 41$
	C	$882 \pm 33$	$909 \pm 29$

In method **C**, contrary to the other two methods,  $\frac{t}{\lambda}$  represents the thickness of the modified Horita plot whose fitting parameters are used to calculate the  $\zeta$ -factors shown in table 3.7. The  $\zeta$ -factor of the light elements (O and C) are determined directly from the fitting parameters. An additional step is necessary to obtain the  $\zeta$ -factor of the heavier elements (Si and Zn). Since the absorption-free k-factor is equal to the quotient of the  $\zeta$ -factor of the light element and the  $\zeta$ -factor of the heavy element, it is possible to calculate one  $\zeta$ -factor if the other is known according to equation 2.14. In order to get the absorption-free k-factor the k-factors at different specimen thicknesses are plotted over the relative thickness and extrapolated to zero-thickness (see figure 3.6 (d)). One drawback here is that the precision of the calculated second  $\zeta$ -factor suffers from the errors of two different fitting methods. This leads to relative errors of about 10%. A benefit is, that additionally to  $\zeta$ -factors, the inelastic mean free path  $\lambda$  of the specimen is determined. The EELS measurement is not influenced by absorption and therefore, method **C** is considered to deliver more reliable results. Especially the  $\zeta$ -factors of the O-K line determined with SiO<sub>2</sub> and ZnO should have similar results and their error margins ought to overlap. Since this is not the case, for both detectors, other error sources need to be contemplated.

**Table 3.7:**  $\zeta$ -factors for K( $\alpha$ )-lines of C, O, Si, Zn and inelastic mean free path  $\lambda$  determined by fitting parameters of the thickness-dependent intensity of the light element (method **C**) measured with the EDX detectors I and II. Errors were determined using single standard deviation.

Specimen	Element	$\zeta$ -factor $\left[ \frac{\text{kg}\cdot\text{electron}}{\text{m}^2\cdot\text{photon}} \right]$		$\lambda$ [nm]	
		Detector I	Detector II	Detector I	Detector II
<b>SiO<sub>2</sub></b>	Si	528 ± 80	496 ± 69	191 ± 12	193 ± 7
	O	509 ± 29	483 ± 19		
<b>ZnO</b>	Zn	1103 ± 89	1286 ± 92	135 ± 4	140 ± 4
	O	416 ± 14	439 ± 14		
<b>SiC</b>	Si	559 ± 66	571 ± 49	123 ± 9	142 ± 9
	C	863 ± 32	899 ± 29		

In figure 3.8, the  $\zeta$ -factors of the oxygen K-line are depicted. The relative error of the single values lies between 3 and 6%. The difference of the determined values are up to approximately 20% at detector I and up to 30% at detector II. While at detector I method **A** and **B** lead to more similar results than method **C**, at detector II it appears to be vice versa. Therefore, no method can be preferred to the other and further error sources need to be considered. The geometry of detector I and II, namely the detector elevation angle, could vary from each other. This fact may lead to different results at the two used detectors.

The observed differences of the Si K $\alpha$ -line  $\zeta$ -factors (figure 3.9) are similar to figure 3.8. The relative errors of the  $\zeta$ -factors determined with method **C** lie between 9 and 15%. Because this relative errors have their origin from two different fitting procedures they appear to be larger than errors obtained with method **A** and **B**.

Figure 3.10 and 3.11 show the obtained  $\zeta$ -factors for the carbon K-line and the zinc K $\alpha$ -line. Here, it is remarkable, that the results for carbon determined with different fitting procedures are more similar. One possible reason is that the difference of absorption of the two involved elements is higher than for the other two used standards. Especially the carbon K line is heavily absorbed in SiC. (see table 3.2). The results at detector II are constantly higher compared to detector I, which could be explained by slightly different solid angles due to small differences of the geometry.

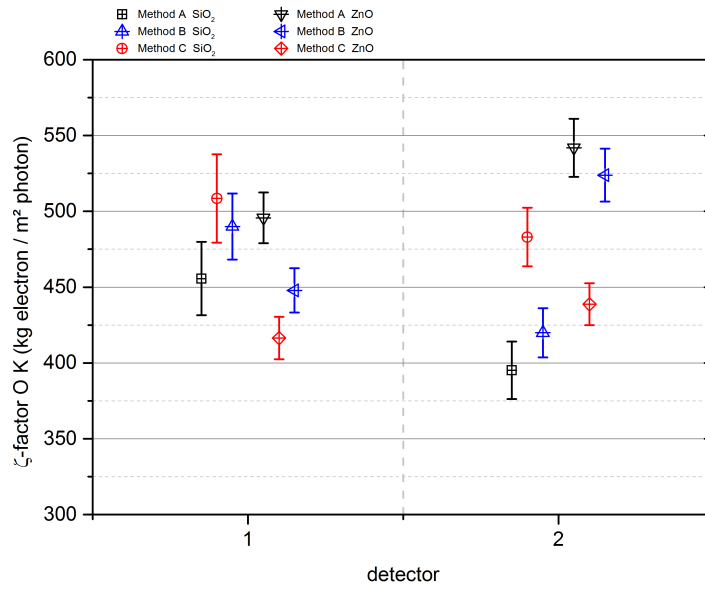


**Figure 3.8:** Summarized values for the  $\zeta$ -factor of the oxygen K-line determined with SiO<sub>2</sub> and ZnO at detector I and II with method **A**, **B** and **C**

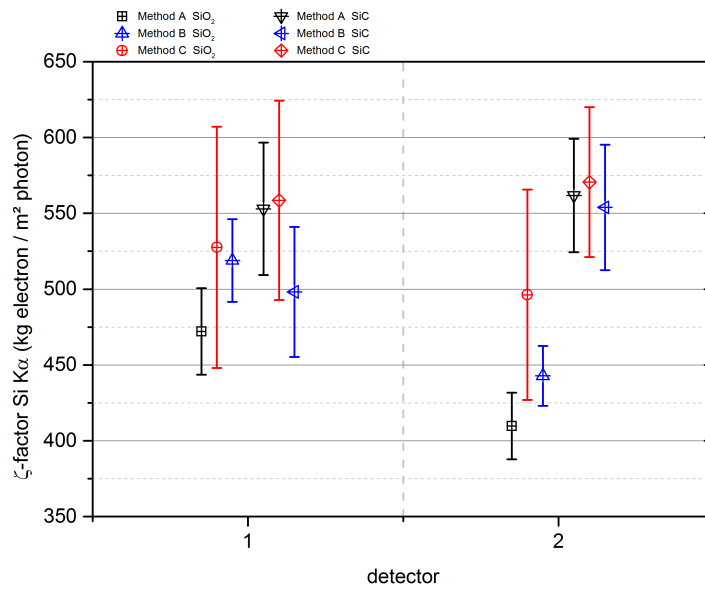


**Figure 3.9:** Summarized values for the  $\zeta$ -factor of the silicon K-line determined with SiO<sub>2</sub> and SiC at detector I and II with method **A**, **B** and **C**

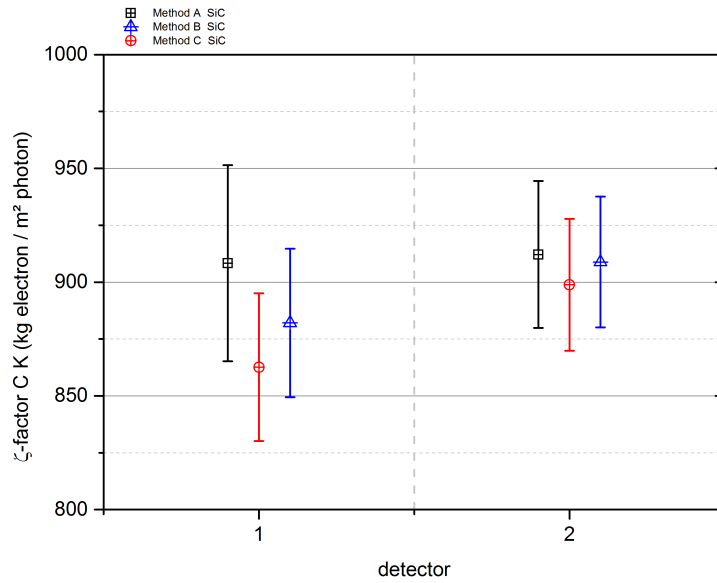


**Figure 3.10:** Summarized values for the  $\zeta$ -factor of the carbon K-line determined with SiC at detector I and II with method **A**, **B** and **C**

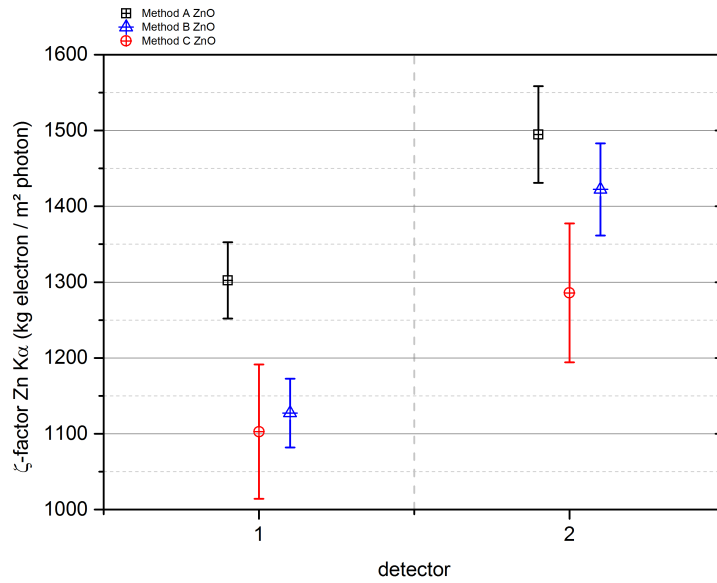


**Figure 3.11:** Summarized values for the  $\zeta$ -factor of the zinc  $K\alpha$ -line determined with ZnO at detector I and II with method **A**, **B** and **C**

Figure 3.12 gives an overview of the determined  $\zeta$ -factors of carbon, oxygen, silicon and zinc. The selected values were determined with method **C** at detector I. The trend of increased  $\zeta$ -factors for high (zinc) and low (carbon) atomic numbers appears to be similar to the behavior Fladischer observed for the same system [18]. While Fladischer's values for light elements were unreliable and highly dependent on the used model for the ionization cross section, in our case, the method is particularly suitable for low atomic numbers. In figure 3.13, the results for the IMFP are illustrated for detector I and II. This parameter should only depend on the specimen itself and not on the detector. Nevertheless,  $\lambda$  is calculated with the take-off angle which depends on the elevation angle of each individual detector. This fact could again explain the continued trend of higher values when measuring with detector II. The IMFP of a specific material can be calculated if the incident-convergence semi-angle, the EELS collection semi-angle and the high voltage are known. Depending on the used models by Malis et al. [13], Iakubovski et al. [19] or Jin et al. [20] different values are obtained. The range of the determined IMFP's of SiO<sub>2</sub>, ZnO and SiC are shown in table 3.8. If we compare the experimentally determined values and the calculated values the IMFP's of ZnO and SiC a nice correspondence can be seen. Although the measured values of SiO<sub>2</sub> are slightly out of the calculated range the determined values of all three specimens seem to be reasonable.

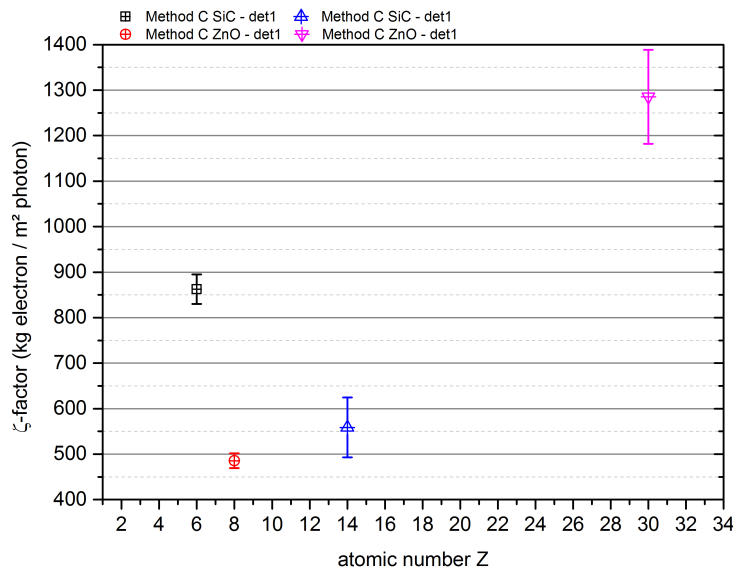


**Figure 3.12:** Values for the  $\zeta$ -factors of carbon K-, oxygen K-, silicon K $\alpha$ - and zinc K $\alpha$ -lines determined with SiC and ZnO at detector I with the  $\frac{t}{\lambda}$ -method

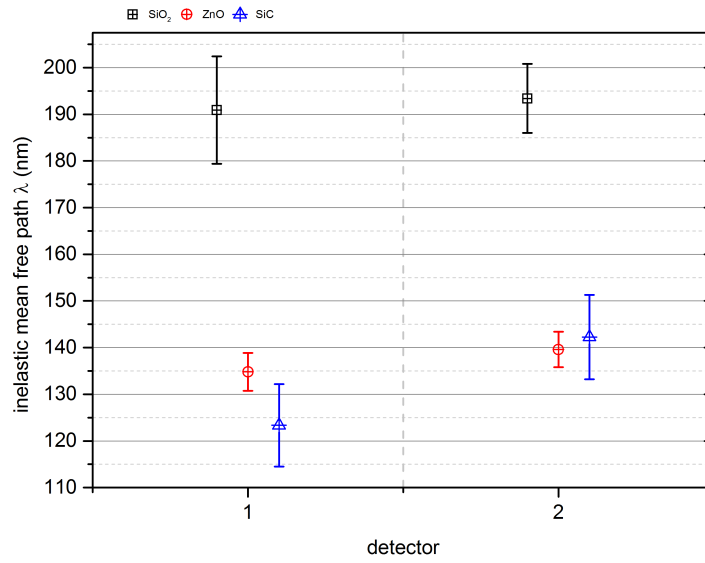


**Figure 3.13:** Inelastic mean free path  $\lambda$  of SiO<sub>2</sub>, ZnO and SiC determined at detector I and II

**Table 3.8:** Calculated inelastic mean free path  $\lambda$  of SiO<sub>2</sub>, ZnO and SiC

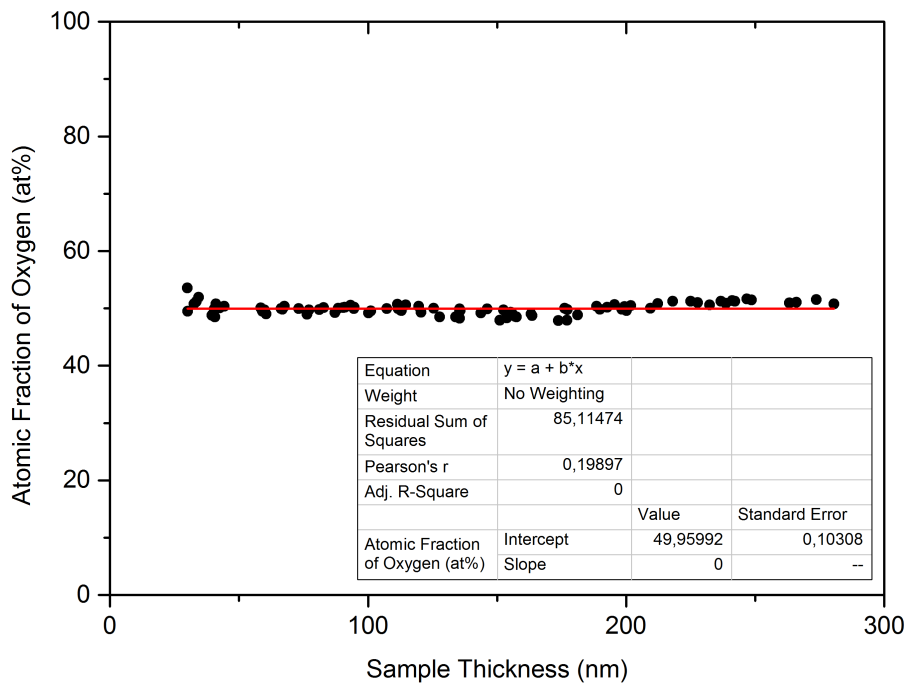
Specimen	range of IMFP $\lambda$ [nm]
<b>SiO<sub>2</sub></b>	139 – 177
<b>ZnO</b>	105 – 147
<b>SiC</b>	120 – 169



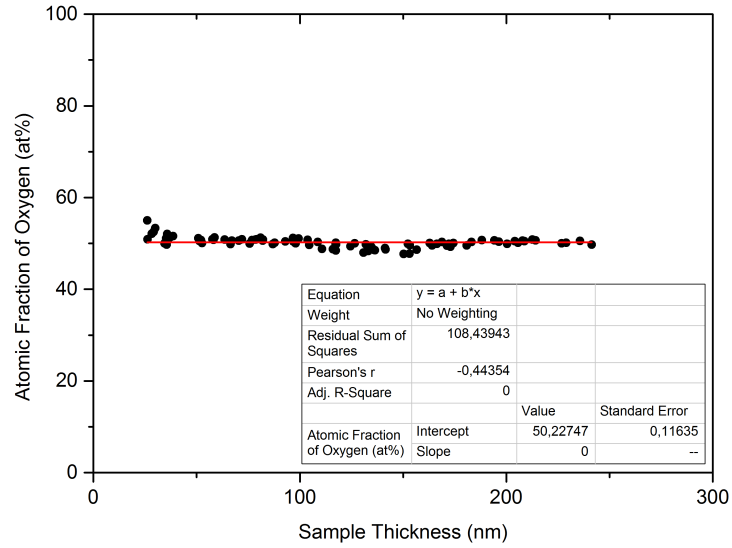
### Evaluation - Quantification

In order to evaluate which method is regarded as most accurate and reliable, the calculated  $\zeta$ -factors were used to perform the quantification by the iterative procedure shown in figure 2.3. This iterative procedure was implemented in a Matlab-script to obtain the elemental concentrations and the mass-thickness of each specimen. The script can be found in the appendix. The input parameters are the measured X-ray intensities at different thicknesses, the determined  $\zeta$ -factors, the electron dose and the take-off angle. Since an absorption correction is applied, in theory, each spectrum should deliver the same result of elemental concentrations.

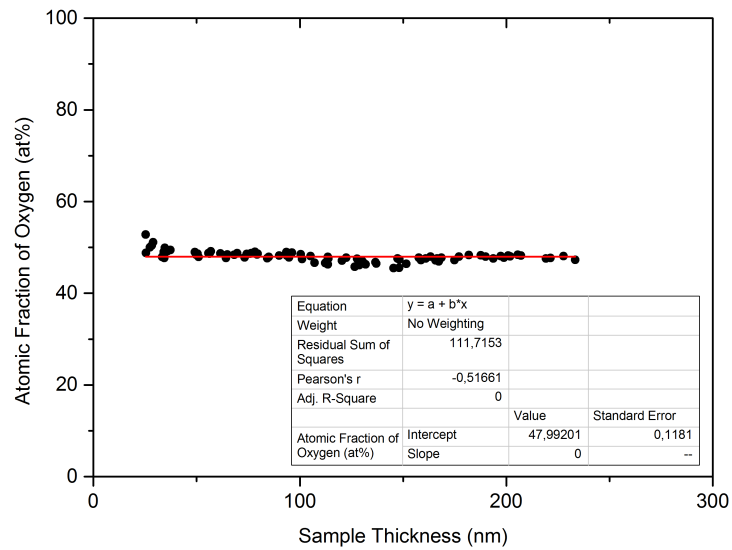
In figure 3.14 the elemental concentration of oxygen in atomic percent (at%) in ZnO is plotted over the specimen thickness. The mass-thickness, as a result of the  $\zeta$ -factor method, gives us the actual specimen thickness if it is divided by the standard's density. A linear, horizontal fit was applied whose intercept parameter gives us the mean value for the elemental concentration. Moreover, the functionality of the absorption correction can be estimated if we compare the deviations of the data-points from the fit at different thicknesses.



(a)



(b)



(c)

**Figure 3.14:** Determination of the atomic fraction of oxygen in **ZnO**. The intercept of the linear fit indicates the mean value of the elemental concentration in at%. The data was acquired at **detector I** and evaluated with  $\zeta$ -factors obtained by method A (a), B (b) and C (c)

The relative error (single standard deviation) of the quantification result of each graph in figure 3.14 is approximately 2%. This indicates that no thickness dependence of the obtained concentrations is observable and thus, the absorption correction was performed successfully.

The atomic concentration of oxygen in ZnO is 50%. The obtained values deviate from the nominal value depending on which  $\zeta$ -factors (method **A**, **B** or **C**) were used for quantification. Method **A** (49.96 at%) and **B** (50.23 at%) are evidently closer to the theoretical value than method **C** (47.99 at%). In this particular case of ZnO, the EELS measurement needed for method **C** seems to be influenced by an additional effect which has to be investigated in more detail in future work, but will not be part of this master thesis.

While in ZnO the deviation from the theoretical concentrations strongly depends on the used method, the results of SiO<sub>2</sub> and SiC have similar values for all three methods (see appendix B for all graphs/results).

Since the result rather depends on the combination of the  $\zeta$ -factors of oxygen and zinc than on their absolute values, it is questionable if an evaluation of the different methods in terms of accuracy is possible. Moreover, in each case, both  $\zeta$ -factors were determined from the same measurement series that has been quantified. Thus, the obtained  $\zeta$ -factors need to be tested on an independent standard to get a reliable verification.



# CHAPTER 4

---

## Conclusion

---

The aim of this Master's thesis was the development of a method to determine  $\zeta$ -factors without explicitly measuring the specimen thickness. This was achieved by using the effect of absorption in a thin film which is related to the film thickness. X-ray absorption can be illustrated by Horita plots where X-ray intensity ratios (k-factors), measured at different specimen thicknesses, are plotted against thickness or a valid measure for thickness  $\frac{t}{\lambda}$ . Motivated by the work of Marvel et al. [15]  $\zeta$ -factors were determined via three different kinds (methods) of Horita plots. Method **A** uses an original Horita plot as described above. In method **B** the absorbed X-ray line is plotted over the non-absorbed X-ray line and in method **C** the absorbed X-ray line is plotted over the relative thickness. For these plots, exponential fits were performed whose fitting parameters were used to determine  $\zeta$ -factors.

The data was acquired with EDXS and EELS measurements on a Titan microscope. The measurements were taken from three different standards: SiO<sub>2</sub>, ZnO and SiC single crystals. Two detectors of the Super-X detector were used individually. The EDX and EEL spectra were measured at different thicknesses. In order to ensure that enough absorption takes place to realize an exponential fit, the MAC of the absorbed X-ray line within the specimen needs to be sufficiently large. We experienced that values of  $\frac{\mu}{\rho} > 400 \text{ kg/m}^2$  are adequate. Additionally, the take-off angle should be minimized which leads to more absorption since the absorption path increases.

The obtained  $\zeta$ -factors of the four X-ray lines of carbon, oxygen, silicon and zinc are similar to the values measured previously by Fladischer [18] and Kraxner [11] achieved with other methods for the same system. The elements oxygen and silicon are present in two specimens and their  $\zeta$ -factors ought to be equal. In order to evaluate the used methods in terms of accuracy and reliability the obtained values were determined independently and compared afterwards. Differences of approximately 20% at detector I and 30% at detector II have been noticed. Although, method **C** is considered to be more accurate than **A** and **B** no trend is observable.

Additionally, the calculated  $\zeta$ -factors were used to quantify the acquired spectra. The absorption correction was successfully applied and mean concentrations near to the theoretical value of the standards were obtained (max.  $\pm 4$  at% difference). Especially, the quantification results of ZnO spectra with  $\zeta$ -factors determined by method **C** differed strongly from the expected value which may be a hint for an additional effect that influences

the EELS measurement. Owing to the fact that the quantification was applied on the spectra which were used to obtain  $\zeta$ -factors in the first place the significance of these results should be handled with care. Moreover, the quantification rather depends on the combination of two  $\zeta$ -factors than on their absolute values. As a next step, the obtained  $\zeta$ -factors could be applied on an independent specimen to evaluate them reliably.

None the less, a  $\zeta$ -factor determination without measuring the specimen thickness is indeed possible. Especially, if there is a high amount of absorption the results of the applied methods seem to be reliable. This can be observed on the results for the  $\zeta$ -factor of the carbon K-line in SiC - their error-margins overlap over a wide range. Hence, an additional EELS measurement is not required to get reliable results. However, if method C is applied the relative thickness needs to be measured. At the cost of an additional EELS measurement the IMFP  $\lambda$  is obtained. The IMFP's of SiO<sub>2</sub>, ZnO and SiC were measured and compared with calculated values. They agreed with each other. On the other hand a further factor of uncertainty has to be considered if an additional measurement is applied. It is emphasized that the newly developed method is especially suitable to determine  $\zeta$ -factors of light elements whose X-ray lines suffer heavily from absorption. This is a major benefit for X-ray quantification since they are present in many chemical compounds. Moreover, the same technique could be applied to any pure element standard for heavy elements which possess high-energy (K, L) and low-energy (L, M, N...) X-ray lines.

---

## Bibliography

---

1. WATANABE, M. and DAVID B. WILLIAMS: ‘The quantitative analysis of thin specimens: a review of progress from the Cliff-Lorimer to the new zeta-factor methods’. *Journal of Microscopy* (2006), vol. 221(2): pp. 89–109 (cit. on pp. [1](#), [6](#), [7](#), [9](#), [10](#)).
2. WILLIAMS, DAVID B. and C. BARRY CARTER: *Transmission electron microscopy: A textbook for materials science*. 2nd ed. New York: Springer, 2008. ISBN: 9780387765006 (cit. on pp. [3](#), [4](#), [6](#), [7](#), [11](#)).
3. RUSS, JOHN C.: *Fundamentals of Energy Dispersive X-ray Analysis: Chapter 6 - X-Ray Absorption*. Butterworths Monographs in Materials. Butterworth-Heinemann, 1984. ISBN: 978-0-408-11031-0. DOI: [10.1016/B978-0-408-11031-0.50009-2](#) (cit. on p. [5](#)).
4. HUBBELL, J. H.: ‘Photon mass attenuation and energy-absorption coefficients’. *The International Journal of Applied Radiation and Isotopes* (1982), vol. 33(11): pp. 1269–1290. ISSN: 0020-708X. DOI: [10.1016/0020-708X\(82\)90248-4](#) (cit. on p. [5](#)).
5. MAHER, D.M., JOY, D.C., ELLINGTON, M.B., ZALUZEC, N.J. & MOCHEL, P.E.: ‘Relative accuracy of k-factor calculations for thin-film X-ray analysis. Analytical Electron Microscopy – 1981 (ed. by R. H. Geiss)’. (1981), vol.: pp. 33–38 (cit. on p. [7](#)).
6. HORITA, ZENJI, SANO TAKESHI, and NEMOTO MINORU: ‘Simplification of X-ray absorption correction in thin-sample quantitative Microanalysis’. *Ultramicroscopy* (1987), vol. 21: pp. 271–276 (cit. on p. [7](#)).
7. GAUVIN, RAYNALD: ‘What remains to be done to allow quantitative X-ray microanalysis performed with EDS to become a true characterization technique?’ *Microscopy and microanalysis : the official journal of Microscopy Society of America, Microbeam Analysis Society, Microscopical Society of Canada* (2012), vol. 18(5): pp. 915–940. DOI: [10.1017/S1431927612001468](#) (cit. on p. [8](#)).
8. KOTHLEITNER, GERALD, WERNER GROGGER, MARTINA DIENSTLEDER, and FERDINAND HOFER: ‘Linking TEM analytical spectroscopies for an assumptionless compositional analysis’. *Microscopy and microanalysis : the official journal of Microscopy Society of America, Microbeam Analysis Society, Microscopical Society of Canada* (2014), vol. 20(3): pp. 678–686. DOI: [10.1017/S1431927614000130](#) (cit. on p. [9](#)).
9. ZANAGA, DANIELE, THOMAS ALTANTZIS, JONATHAN SANCTORUM, BERT FREITAG, and SARA BALS: ‘An alternative approach for Zeta-factor measurement using pure element nanoparticles’. *Ultramicroscopy* (2016), vol. 164: pp. 11–16. DOI: [10.1016/j.ultramicro.2016.03.002](#) (cit. on p. [9](#)).

10. H. H. PATTEE, V. E. COSSLETT, ARNE ENGSTRÖM, ed.: *X-ray Optics and X-ray Microanalysis: A Method for Calculating the Absorption Correction in Electron-Probe Microanalysis*. Academic Press, 1963. ISBN: 978-1-4832-3322-2 (cit. on p. 10).
11. KRAXNER, JOHANNA: ‘Analytical TEM of organic electronics with a special focus on EDXS and geometry aspects’. PhD Thesis. Graz: TU Graz, 2017 (cit. on pp. 11, 28, 30, 41).
12. GONG, H. and F. W. SCHAPINK: ‘Foil-thickness determination from zone-axis CBED patterns and TEM images for a GaAs/AlAs multilayer in plan view’. *Ultramicroscopy* (1992), vol. 41(4): pp. 375–385. DOI: [10.1016/0304-3991\(92\)90217-8](https://doi.org/10.1016/0304-3991(92)90217-8) (cit. on p. 11).
13. MALIS, T., S. C. CHENG, and R. F. EGERTON: ‘EELS log-ratio technique for specimen-thickness measurement in the TEM’. *Journal of Electron Microscopy Technique* (1988), vol. 8(2): pp. 193–200. ISSN: 1553-0817. DOI: [10.1002/jemt.1060080206](https://doi.org/10.1002/jemt.1060080206) (cit. on pp. 11, 35).
14. HORITA, ZENJI, SANO TAKESHI, and NEMOTO MINORU: ‘Extrapolation method for the determination of Cliff-Lorimer  $k_{AB}$  factors at zero foil thickness’. *Journal of Microscopy* (1986), vol. 143(3): pp. 215–231 (cit. on pp. 11, 12).
15. MARVEL, C. J., K. D. BEHLER, J. C. LASALVIA, V. DOMNICH, R. A. HABER, M. WATANABE, and M. P. HARMER: ‘Extending zeta-factor microanalysis to boron-rich ceramics: Quantification of bulk stoichiometry and grain boundary composition’. *Ultramicroscopy* (2019), vol. 202: pp. 163–172. DOI: [10.1016/j.ultramic.2019.04.008](https://doi.org/10.1016/j.ultramic.2019.04.008) (cit. on pp. 12, 13, 41).
16. NATIONAL INSTITUTE OF STANDARDS AND TECHNOLOGY: *NIST X-Ray Form Factor, Atten. Scatt. Tables Form Page*. 2016. URL: <https://physics.nist.gov/PhysRefData/FFast/html/form.html> (cit. on p. 20).
17. SCHLOSSMACHER, P., D. O. KLENOV, B. FREITAG, S. VON HARRACH, AND A. STEINBACH: ‘Nanoscale Chemical Compositional Analysis with an Innovative S/TEM-EDX System’. *Microscopy and Analysis* (2010), vol. 24(7): pp. 5–8 (cit. on p. 22).
18. FLADISCHER, STEFANIE: ‘Application of new EDXS quantification schemes in TEM to organic semiconducting devices’. PhD thesis. Graz: TU Graz, 2013 (cit. on pp. 30, 35, 41).
19. IAKOUBOVSKII, K., K. MITSUISHI, Y. NAKAYAMA, and K. FURUYA: ‘Thickness measurements with electron energy loss spectroscopy’. *Microscopy research and technique* (2008), vol. 71(8): pp. 626–631. DOI: [10.1002/jemt.20597](https://doi.org/10.1002/jemt.20597) (cit. on p. 35).
20. JIN, Q. and D. LI: ‘Determining Inelastic Mean Free Path by Electron Energy Loss Spectroscopy’. *Microscopy and Microanalysis* (2006), vol. 12(S02): pp. 1186–1187. ISSN: 1431-9276. DOI: [10.1017/S1431927606061770](https://doi.org/10.1017/S1431927606061770) (cit. on p. 35).



---

## List of Figures

---

2.1	The ionization process. An inner (K) shell electron is ejected from the atom by a high-energy electron. When the hole in the K-shell is filled by an electron from the L-shell, characteristic ( $K\alpha$ ) X-ray emission occurs. The incident electron loses energy and continues its way through the specimen. (taken from D. B. Williams et al. [2]) . . . . .	3
2.2	Possible electron transitions that give rise to K, L and M characteristic X-rays. Not all of them are detectable by the EDXS in the TEM. (taken from D. B. Williams et al. [2]) . . . . .	4
2.3	A flow chart of the quantification procedure in the $\zeta$ -factor method with the X-ray absorption correction. (taken from Watanabe et al. [1]) . . . . .	10
2.4	Relationship between the specimen thickness $t$ and the absorption path length $t \cdot \text{cosec}\alpha_{TO}$ , for a take-off angle $\alpha_{TO}$ . (taken from D. B. Williams et al. [2]) . . . . .	11
2.5	Example of a Horita plot showing measuring points at different thicknesses. The thickness is represented by the silicon $K\alpha$ -line intensity of a SiC crystal. The intersection of the exponential fit with the ordinate indicates the absorption-free k-factor. (taken from Marvel et al. [15]) . . . . .	12
3.1	SiO <sub>2</sub> lamella mounted on an Omniprobe grid in top-position, SE image taken during FIB preparation . . . . .	21
3.2	Schematic of the Super-X geometry: Four SDD detectors are arranged symmetrically around the sample (taken from Schlossmacher et al. [17]). . . . .	22
3.3	ZnO lamella with indicated measurement points . . . . .	23
3.4	An original EDX spectrum of SiO <sub>2</sub> with fitted background . . . . .	24
3.5	Orientation of the Omniprobe grid in the Super-X holder for detector I: (a) from top, (b) from below . . . . .	25
3.6	Graphs performed for $\zeta$ -factor determination of ZnO at detector I; (a) k-factor dependence over Zn $K\alpha$ Intensity; (b) O K Intensity dependence over Zn $K\alpha$ Intensity; (c) O K Intensity dependence over $\frac{t}{\lambda}$ ; (d) k-factor dependence over $\frac{t}{\lambda}$ . . . . .	28
3.7	Angle measurement of the mounted ZnO lamella with respect to the Omniprobe grid: (a) shows the angle in $\alpha$ direction ( $\alpha = 0^\circ$ ), (b) in $\beta$ direction ( $\beta = 1.4^\circ$ ). . . . .	29
3.8	Summarized values for the $\zeta$ -factor of the oxygen K-line determined with SiO <sub>2</sub> and ZnO at detector I and II with method <b>A</b> , <b>B</b> and <b>C</b> . . . . .	33

3.9	Summarized values for the $\zeta$ -factor of the silicon K-line determined with SiO <sub>2</sub> and SiC at detector I and II with method <b>A</b> , <b>B</b> and <b>C</b> . . . . .	33
3.10	Summarized values for the $\zeta$ -factor of the carbon K-line determined with SiC at detector I and II with method <b>A</b> , <b>B</b> and <b>C</b> . . . . .	34
3.11	Summarized values for the $\zeta$ -factor of the zinc K $\alpha$ -line determined with ZnO at detector I and II with method <b>A</b> , <b>B</b> and <b>C</b> . . . . .	34
3.12	Values for the $\zeta$ -factors of carbon K-, oxygen K-, silicon K $\alpha$ - and zinc K $\alpha$ -lines determined with SiC and ZnO at detector I with the $\frac{t}{\lambda}$ -method . . . . .	35
3.13	Inelastic mean free path $\lambda$ of SiO <sub>2</sub> , ZnO and SiC determined at detector I and II . . . . .	36
3.14	Determination of the atomic fraction of oxygen in <b>ZnO</b> . The intercept of the linear fit indicates the mean value of the elemental concentration in at%. The data was acquired at <b>detector I</b> and evaluated with $\zeta$ -factors obtained by method A (a), B (b) and C (c) . . . . .	38
B.1	Graphs performed for $\zeta$ -factor determination of <b>ZnO at detector II</b> ; (a) k-factor dependence over Zn K $\alpha$ intensity; (b) O-K intensity dependence over Zn K $\alpha$ intensity; (c) O-K intensity dependence over $\frac{t}{\lambda}$ ; (d) k-factor dependence over $\frac{t}{\lambda}$ . . . . .	61
B.2	Graphs performed for $\zeta$ -factor determination of <b>SiO<sub>2</sub> at detector I</b> ; (a) k-factor dependence over Si-K intensity; (b) O-K intensity dependence over Si-K Intensity; (c) O-K intensity dependence over $\frac{t}{\lambda}$ ; (d) k-factor dependence over $\frac{t}{\lambda}$ . . . . .	62
B.3	Graphs performed for $\zeta$ -factor determination of <b>SiO<sub>2</sub> at detector II</b> ; (a) k-factor dependence over Si-K intensity; (b) O-K intensity dependence over Si-K intensity; (c) O-K intensity dependence over $\frac{t}{\lambda}$ ; (d) k-factor dependence over $\frac{t}{\lambda}$ . . . . .	63
B.4	Graphs performed for $\zeta$ -factor determination of <b>SiC at detector I</b> ; (a) k-factor dependence over Si-K intensity; (b) C-K intensity dependence over Si-K intensity; (c) C-K intensity dependence over $\frac{t}{\lambda}$ ; (d) k-factor dependence over $\frac{t}{\lambda}$ . . . . .	63
B.5	Graphs performed for $\zeta$ -factor determination of <b>SiC at detector II</b> ; (a) k-factor dependence over Si-K intensity; (b) C-K intensity dependence over Si-K intensity; (c) C-K intensity dependence over $\frac{t}{\lambda}$ ; (d) k-factor dependence over $\frac{t}{\lambda}$ . . . . .	64
B.6	Determination of the atomic fraction of oxygen in <b>ZnO</b> . The intercept of the linear fit indicates the mean value of the elemental concentration in at%. The data was acquired at <b>detector II</b> and evaluated with $\zeta$ -factors obtained by method A (a), B (b) and C (c). . . . .	65
B.7	Determination of the atomic fraction of oxygen in <b>SiO<sub>2</sub></b> . The intercept of the linear fit indicates the mean value of the elemental concentration in at%. The data was acquired at <b>detector I</b> and evaluated with $\zeta$ -factors obtained by method A (a), B (b) and C (c). . . . .	66

- 
- B.8 Determination of the atomic fraction of oxygen in **SiO<sub>2</sub>**. The intercept of the linear fit indicates the mean value of the elemental concentration in at%. The data was acquired at **detector II** and evaluated with  $\zeta$ -factors obtained by method A (a), B (b) and C (c). . . . . 67
- B.9 Determination of the atomic fraction of carbon in **SiC**. The intercept of the linear fit indicates the mean value of the elemental concentration in at%. The data was acquired at **detector I** and evaluated with  $\zeta$ -factors obtained by method A (a), B (b) and C (c). . . . . 67
- B.10 Determination of the atomic fraction of carbon in **SiC**. The intercept of the linear fit indicates the mean value of the elemental concentration in at%. The data was acquired at **detector II** and evaluated with  $\zeta$ -factors obtained by method A (a), B (b) and C (c). . . . . 68



---

## List of Tables

---

3.1	Materials used for the acquisition of EDXS and EELS spectrum images c...concentration in percentage by mass [wt%] $\rho$ ...density [g/cm <sup>3</sup> ] . . . . .	20
3.2	MACs for Si and O in SiO <sub>2</sub> , Zn and O in ZnO, Si and C in SiC, values taken for the K( $\alpha$ ) lines, source: NIST-database [16] . . . . .	20
3.3	Measurement parameters . . . . .	22
3.4	Take-off angle and electron dose for each measured specimen at the detectors I and II . . . . .	29
3.5	$\zeta$ -factors for K( $\alpha$ )-lines of C, O, Si and Zn determined from fitting parameters of the thickness dependent k-factor (method <b>A</b> ) measured with the EDX detectors I and II. Errors were determined using single standard deviation. . .	30
3.6	$\zeta$ -factors for K( $\alpha$ )-lines of C, O, Si and Zn determined by fitting parameters of the thickness-dependent intensity (method <b>B</b> ) measured with the EDX detectors I and II. Errors were determined using single standard deviation. . .	31
3.7	$\zeta$ -factors for K( $\alpha$ )-lines of C, O, Si, Zn and inelastic mean free path $\lambda$ determined by fitting parameters of the thickness-dependent intensity of the light element (method <b>C</b> ) measured with the EDX detectors I and II. Errors were determined using single standard deviation. . . . .	32
3.8	Calculated inelastic mean free path $\lambda$ of SiO <sub>2</sub> , ZnO and SiC . . . . .	36



# A Used Matlab scripts

## A.1 Matlab script to evaluate EDX-spectra in terms of peak intensities

The written Matlab script has to be modified for each specimen. The core of the script are the built-in functions *findpeaks.m* and *peakfit.m* which determine the location of the gauss-peaks and evaluate them in terms of intensity. The background was fitted with a polynomial function. The provided data for the fit was created by averaging over five channels next to the peaks. These locations were determined in Digital Micrograph. The file from DM was read by the function *ReadDMFile2Dto4D.m*. The following source code was used to calculate the intensities of the oxygen K and silicon K $\alpha$  peaks of the SiO<sub>2</sub> lamella.

```
1 close all
2 clear all
3
4 %read the DM-file with the function ReadDMFile2Dto4D
5 filename = 'C:\UNI\Master\Masterarbeit\Messungen\TITAN\SiC Lamelle Det1\SI-005\
EDS Spectrum Image.dm4';
6
7 %write the data into the matrix 'SPECTRUM'
8 [spec, scales, units, origins, bn_scale, bn_origin, bn_unit] = ReadDMFile2Dto4D(
filename);
9 spec = double(spec)
10
11 SPECTRUM = num2cell(spec)
12 %%
13
14 %subtract the first part of the spectrum to align the energy scale
15 %(the spectra provided by DM start at -475 eV)
16 for i=1:96
17 SPECTRUM(1,:)=[]
18 i+1;
19 end
20
21 channels = length(SPECTRUM);
22 %%
23 %choose the spectra of the measurment series
24 for j=2:11
25
26 for i=1:(channels)
27     intensities(i)=(SPECTRUM{i,j});
28 end
29
```

```
30 dispersion = 5e-3; %kev/channel
31 energy = 0:dispersion:(channels-1).*dispersion;
32 %%
33
34 % Background Model SiO2:
35
36 %values of background window in eV (taken from Digital Micrograph)
37
38 eVbdx1=144;
39 eVbdx2=354;
40 eVbdx3=664;
41 eVbdx4=1579;
42 eVbdx5=1949;
43 eVbdx6=7789;
44 eVbdx7=9574;
45 eVbdx8=19989;
46
47 %values of background window in channels
48
49 bdx1=28;
50 bdx2=70;
51 bdx3=132;
52 bdx4=315;
53 bdx5=389;
54 bdx6=1557;
55 bdx7=1914;
56 bdx8=3998;
57
58 %mean value_counts of 5 channels (+-2 of background window value)
59
60 bdy1=(intensities(bdx1-2)+intensities(bdx1-1)+intensities(bdx1)+intensities(bdx1
+1)+intensities(bdx1+2))/5;
61 bdy2=(intensities(bdx2-2)+intensities(bdx2-1)+intensities(bdx2)+intensities(bdx2
+1)+intensities(bdx2+2))/5;
62 bdy3=(intensities(bdx3-2)+intensities(bdx3-1)+intensities(bdx3)+intensities(bdx3
+1)+intensities(bdx3+2))/5;
63 bdy4=(intensities(bdx4-2)+intensities(bdx4-1)+intensities(bdx4)+intensities(bdx4
+1)+intensities(bdx4+2))/5;
64 bdy5=(intensities(bdx5-2)+intensities(bdx5-1)+intensities(bdx5)+intensities(bdx5
+1)+intensities(bdx5+2))/5;
65 bdy6=(intensities(bdx6-2)+intensities(bdx6-1)+intensities(bdx6)+intensities(bdx6
+1)+intensities(bdx6+2))/5;
66 bdy7=(intensities(bdx7-2)+intensities(bdx7-1)+intensities(bdx7)+intensities(bdx7
+1)+intensities(bdx7+2))/5;
67 bdy8=(intensities(bdx8-2)+intensities(bdx8-1)+intensities(bdx8)+intensities(bdx8
+1)+intensities(bdx8+2))/5;
68
69 bkgrddata = [eps, eps; eVbdx1, bdy1; eVbdx2, bdy2; eVbdx3, bdy3; eVbdx4, bdy4; eVbdx5, bdy5;
eVbdx6, bdy6; eVbdx7, bdy7; eVbdx8, bdy8];
```



```
70 bkgrrdata(:,1) = bkgrrdata(:,1).*1e-3;
71 %%
72 %
73 % % Background Model Zn0:
74 %
75 % %values of background window in eV
76 %
77 % eVbdx1=144;
78 % eVbdx2=354;
79 % eVbdx3=629;
80 % eVbdx4=779;
81 % eVbdx5=1244;
82 % eVbdx6=7729;
83 % eVbdx7=8199;
84 % eVbdx8=8394;
85 % eVbdx9=8999;
86 % eVbdx10=9347;
87 % eVbdx11=9849;
88 % eVbdx12=19989;
89 %
90 % %values of background window in channels
91 %
92 % bdx1=28;
93 % bdx2=70;
94 % bdx3=132;
95 % bdx4=155;
96 % bdx5=248;
97 % bdx6=1545;
98 % bdx7=1639;
99 % bdx8=1678;
100 % bdx9=1799;
101 % bdx10=1874;
102 % bdx11=1969;
103 % bdx12=3998;
104 %
105 % %mean value_counts of 5 channels (+-2 of background window value)
106 %
107 % bdy1=(intensities(bdx1-2)+intensities(bdx1-1)+intensities(bdx1)+intensities(
bdx1+1)+intensities(bdx1+2))/5;
108 % bdy2=(intensities(bdx2-2)+intensities(bdx2-1)+intensities(bdx2)+intensities(
bdx2+1)+intensities(bdx2+2))/5;
109 % bdy3=(intensities(bdx3-2)+intensities(bdx3-1)+intensities(bdx3)+intensities(
bdx3+1)+intensities(bdx3+2))/5;
110 % bdy4=(intensities(bdx4-2)+intensities(bdx4-1)+intensities(bdx4)+intensities(
bdx4+1)+intensities(bdx4+2))/5;
111 % bdy5=(intensities(bdx5-2)+intensities(bdx5-1)+intensities(bdx5)+intensities(
bdx5+1)+intensities(bdx5+2))/5;
112 % bdy6=(intensities(bdx6-2)+intensities(bdx6-1)+intensities(bdx6)+intensities(
bdx6+1)+intensities(bdx6+2))/5;
```

```
113 % bdy7=(intensities(bdx7-2)+intensities(bdx7-1)+intensities(bdx7)+intensities(
114 bdx7+1)+intensities(bdx7+2))/5;
114 % bdy8=(intensities(bdx8-2)+intensities(bdx8-1)+intensities(bdx8)+intensities(
115 bdx8+1)+intensities(bdx8+2))/5;
115 % bdy9=(intensities(bdx9-2)+intensities(bdx9-1)+intensities(bdx9)+intensities(
116 bdx9+1)+intensities(bdx9+2))/5;
116 % bdy10=(intensities(bdx10-2)+intensities(bdx10-1)+intensities(bdx10)+intensities
117 (bdx10+1)+intensities(bdx10+2))/5;
117 % bdy11=(intensities(bdx11-2)+intensities(bdx11-1)+intensities(bdx11)+intensities
118 (bdx11+1)+intensities(bdx11+2))/5;
118 % bdy12=(intensities(bdx12-2)+intensities(bdx12-1)+intensities(bdx12)+intensities
119 (bdx12+1)+intensities(bdx12+2))/5;
119 %
120 % bkgrrdata = [eps,eps;eVbdx1,bdy1;eVbdx2,bdy2;eVbdx3,bdy3;eVbdx4,bdy4;eVbdx5,
121 bdy5;eVbdx6,bdy6;eVbdx7,bdy7;eVbdx8,bdy8;eVbdx9,bdy9;eVbdx10,bdy10;eVbdx11,bdy11;
122 eVbdx12,bdy12];
123 %
124 % % Background Model SiC:
125 %
126 % %values of background window in eV
127 %
128 % eVbdx1=124;
129 % eVbdx2=179;
130 % eVbdx3=389;
131 % eVbdx4=1584;
132 % eVbdx5=1934;
133 % eVbdx6=7929;
134 % eVbdx7=8189;
135 % eVbdx8=19989;
136 %
137 %
138 % %values of background window in channels
139 %
140 % bdx1=24;
141 % bdx2=35;
142 % bdx3=77;
143 % bdx4=316;
144 % bdx5=386;
145 % bdx6=1585;
146 % bdx7=1637;
147 % bdx8=3998;
148 %
149 %
150 % %mean value_counts of 5 channels (+-2 of background window value)
151 %
152 % bdy1=(intensities(bdx1-2)+intensities(bdx1-1)+intensities(bdx1)+intensities(
bdx1+1)+intensities(bdx1+2))/5;
```

```
153 % bdy2=(intensities(bdx2-2)+intensities(bdx2-1)+intensities(bdx2)+intensities(
bdx2+1)+intensities(bdx2+2))/5;
154 % bdy3=(intensities(bdx3-2)+intensities(bdx3-1)+intensities(bdx3)+intensities(
bdx3+1)+intensities(bdx3+2))/5;
155 % bdy4=(intensities(bdx4-2)+intensities(bdx4-1)+intensities(bdx4)+intensities(
bdx4+1)+intensities(bdx4+2))/5;
156 % bdy5=(intensities(bdx5-2)+intensities(bdx5-1)+intensities(bdx5)+intensities(
bdx5+1)+intensities(bdx5+2))/5;
157 % bdy6=(intensities(bdx6-2)+intensities(bdx6-1)+intensities(bdx6)+intensities(
bdx6+1)+intensities(bdx6+2))/5;
158 % bdy7=(intensities(bdx7-2)+intensities(bdx7-1)+intensities(bdx7)+intensities(
bdx7+1)+intensities(bdx7+2))/5;
159 % bdy8=(intensities(bdx8-2)+intensities(bdx8-1)+intensities(bdx8)+intensities(
bdx8+1)+intensities(bdx8+2))/5;
160 %
161 %
162 % bkgrddata = [eps,eps;eVbdx1,bdy1;eVbdx2,bdy2;eVbdx3,bdy3;eVbdx4,bdy4;eVbdx5,
bdy5;eVbdx6,bdy6;eVbdx7,bdy7;eVbdx8,bdy8];
163 % bkgrddata(:,1) = bkgrddata(:,1).*1e-3;
164 %%
165 %
166 % approximate background with spline interpolation:
167 figure;
168 plot(energy,intensities);
169 hold on
170         backgrnd_interpy = interp1(bkgrddata(:,1),bkgrddata(:,2),energy,'pchip'
);
171 plot(bkgrddata(:,1),bkgrddata(:,2),'o',energy,backgrnd_interpy,':.');
172 hold on
173 title('Original spectrum with fitted background');
174 xlabel('Energy [keV]');
175 ylabel('Intensity [counts]');
176 legend('Original Spectrum','Background Data','Fitted Background')
177
178 %%
179
180 % remove background from original spectrum:
181 peaksonly = intensities - backgrnd_interpy;
182 %
183 % estimate peak positions:
184 %findpeaks: gives back the positions of the peaks in the spectrum
185 [peakheights,peakpos] = findpeaks(peaksonly,energy,'MinPeakDistance',0.05,'
MinPeakHeight',300);
186
187 peakdistances = diff(peakpos);
188 count = 1:length(peakpos);
189 for i=1:length(peakdistances)
190     if peakdistances(i)<0.1
191         count(i) = count(i) - 1;
```

```
192     end
193 end
194 peakheights;
195 peakpos;
196 figure;
197 plot(energy,peaksonly);
198 hold on
199 plot(peakpos,peakheights,'o');
200 hold off
201 title('Background corrected spectrum');
202 xlabel('Energy [keV]');
203 ylabel('Intensity [counts]');
204 %%
205
206 % fit peaks (with manual peakpositions):
207 peakpos = 0.525; %position of oxygen K-alpha peak
208 window = 0.4;
209 [FitResults(1,:), ~, ~, ~, xi, yi, ~] = peakfit([energy;peaksonly],peakpos>window
);
210 %see: https://terpconnect.umd.edu/~toh/spectrum/InteractivePeakFitter.htm#command
211
212 peakpos = 1.74; %position of silicon K-alpha peak
213 [FitResults(2,:), ~, ~, ~, xi, yi, ~] = peakfit([energy;peaksonly],peakpos>window
);
214
215 % peakpos = 9.115; %position of zinc K-alpha peak
216 % [FitResults(3,:), ~, ~, ~, xi, yi, ~] = peakfit([energy;peaksonly],peakpos,
>window);
217
218 % peakpos = 0.745; %position of carbon K-alpha peak
219 % [FitResults(3,:), ~, ~, ~, xi, yi, ~] = peakfit([energy;peaksonly],peakpos,
>window);
220
221
222 %%
223
224 % calculate gaussians with above fitting constants:
225
226 for i=1:size(FitResults,1)
227
228     area = FitResults(i,j);
229     calculatedInt(i) = area/dispersion;
230
231 %write the calculated intensities into the matrix IntResults
232     IntResults(5,i)=calculatedInt(i);
233
234 end
235
236 end
```

## A.2 Matlab script to quantify EDX-spectra using the $\zeta$ -factor method

The written Matlab script has to be modified for each specimen and measurement series in terms of input parameters and elemental MACs. The input and output parameters are listed in the first couple of lines. According to figure 2.3 an iterative process is realized. The convergence criteria is chosen at 0.001 %wt for the determined concentrations and at  $10^{-12}$  kg/m<sup>2</sup> (corresponds to approximately 0.01 nm absolute specimen thickness) for the mass-thickness. About 15 iteration steps were necessary to obtain the final result.

```

1 %% Zeta-factor quantification for a BINARY system
2 % written for Nikolaus Rauch by Judith Lammer 27.3.2020
3
4 %output parameters of this script are:
5 %  rhot... rho*t = mass thickness
6 %  c_a... concentration [wt%] of the low-energy element
7 %  c_b... concentration [wt%] of the high-energy element
8
9 % type in all parameters here and load your intensity file. If you run the script
  afterwards, the function
10 % zetafactorquantification.m (below) will perform the quantification for
11 % all your intensities.
12 % NOTE: current, acquisition time, elements and MACs are assumed to be the
13 % same for ALL intensities!
14
15 %% Input parameters
16
17 %  D... dose [electrons] (if not known type in cur and tau)
18 %  cur... current [A] (ATTENTION: if dose is already known, set to 1)
19 %  tau... live time [s] (ATTENTION: if dose is already known, set to 1)
20 %  alpha... take-off angle [degr]
21 %  zet_a... zeta-factor of the low-energy element
22 %  zet_b... zeta-factor of the higher-energy element
23 %  murrho_a... MACspec [cm2/g] of the low-energy X-ray line
24 %  murrho_b... MACspec [cm2/g] of the higher-energy X-ray line
25 %  I... matrix of all intensities als xlsx-file: first column low-energy X-ray
  line, second column higher-energy X-ray line
26
27 %dose (if known):
28 D=118198578097.60;
29 %if dose is not known, type in current and live time:
30 cur = 1; %measured current [A], IF NOT USED SET TO 1!!!!
31 tau = 1; %acquisition time [s] -> live time
32
33 %type in take-off angle
34 alpha = 24.39019608;
35
36 %EDX specific parameters:
37 %zeta-factors
38 zet_a = 545.2336555; % O-K
39 zet_b = 1432.5230592; % Zn-K

```

```

40 |
41 | %elemental MACs (ZnO)
42 | murho_a = 112.149336497841; % O-K in O -> MACspec [m^2/kg]
43 | murho_b = 576.089233275353; % O-K in Zn -> MACspec [m^2/kg]
44 | murho_c = 0.888200755699; % Zn-K in O -> MACspec [m^2/kg]
45 | murho_d = 4.620148790967; % Zn-K in Zn -> MACspec [m^2/kg]
46 |
47 | %elemental MACs (SiO2)
48 | % murho_a = 112.149336497841; % O-K in O -> MACspec [m^2/kg]
49 | % murho_b = 754.2279762; % O-K in Si -> MACspec [m^2/kg]
50 | % murho_c = 97.09024494; % Si-K in O -> MACspec [m^2/kg]
51 | % murho_d = 32.48850367; % Si-K in Si -> MACspec [m^2/kg]
52 | %
53 | %elemental MACs (SiC)
54 | % murho_a = 231.2153508; % C-K in C -> MACspec [m^2/kg]
55 | % murho_b = 3416.858008; % C-K in Si -> MACspec [m^2/kg]
56 | % murho_c = 41.71792322; % Si-K in C -> MACspec [m^2/kg]
57 | % murho_d = 32.48850367; % Si-K in Si -> MACspec [m^2/kg]
58 |
59 | %read in Excelfile with intensities: first column low-energy X-ray line,
60 | %second column higher-energy X-ray line; Attention: readtable sets the
61 | %first row as column description (O-K-int, Zn-K-int), so make sure there
62 | %is one in your Excelsheet!
63 | I = readtable('C:\UNI\Master\Masterarbeit\Berechnungen\Quantifizierung\
int_ZnO_det1.xlsx');
64 |
65 | %% ZETA-FACTOR-Quantification: run the function
66 | [rhot, c_a, c_b] = zetaquantification(D,cur,tau,alpha,zet_a,zet_b,murho_a,murho_b
,murho_c,murho_d,I);
67 |
68 | %% saving results to xlsx-file
69 | header = {'rho*t', 'conc_low-energy', 'conc_high-energy'}; %names for columns in
Excelsheet (first row!)
70 | result = [rhot, c_a, c_b]; %data for Exelsheet in one Matrix
71 | filename = 'C:\UNI\Master\Masterarbeit\Berechnungen\Quantifizierung\ZnO\Detektor
1\test-higher-dose.xlsx'; %location and filename of Excelsheet
72 |
73 | xlswrite(filename, header, 1,'A1:C1'); %saving first row in Excelsheet
74 | xlswrite(filename, result, 1,'A2'); %saving data in Excelsheet (starting with 2nd
row)

```

```

1 | %% This function performs a zeta-Faktor quantification with a binary system
2 |
3 | %output parameters:
4 | % rhot... rho*t = mass thickness
5 | % c_a... concentration [wt%] of the low-energy element
6 | % c_b... concentration [wt%] of the high-energy element
7 |
8 | %input parameters:

```

```
9 % D... dose [electrons] (if not known type in cur and tau)
10 % cur... current [A] (ATTENTION: if dose is already known, set to 1)
11 % tau... live time [s] (ATTENTION: if dose is already known, set to 1)
12 % alpha... take-off angle [degr]
13 % zet_a... zeta-factor of the low-energy element
14 % zet_b... zeta-factor of the higher-energy element
15 % murrho_a... MACspec [cm2/g] of the low-energy X-ray line
16 % murrho_b... MACspec [cm2/g] of the higher-energy X-ray line
17 % I... matrix of all intensities: first column low-energy X-ray line,
18 %                               second column higher-energy X-ray line
19
20 function [rhot, c_a, c_b]=zetaquantification(D,cur,tau,alpha,zet_a,zet_b,murho_a,
murho_b,murho_c,murho_d, I)
21 %% section for playing around with just one spectrum - just for checking the code
- please ignore it
22
23 %type in acquisition parameters:
24
25 %if dose is known, type in dose:
26 %D=107453252816.001;
27
28 %if dose is not known, type in current and live time:
29 %cur = 1; %measured current [A], IF NOT USED SET TO 1!!!!
30 %tau = 1; %acquisition time [s] -> live time
31
32 % type in take-off angle
33 %alpha=36.71;
34
35 %type in EDX specific parameters:
36 %n=2;
37
38 % type in zeta-factors
39 %zet_a = 549.953; % O-K
40 %zet_b = 1455.45; % Zn-K
41
42 % type in MAC for the specific energy in the material
43 %murho_a = 4848.90; % O-K in ZnO -> MACspec [cm2/g]
44 %murho_b = 38.87; % Zn-K in ZnO -> MACspec [cm2/g]
45
46 %type in intensities
47 %intensities from lowest to highest energy
48 %I_a = 7184.643657; % O-K intensity
49 %I_b = 10948.62689; % Zn-K intensity
50
51 %% one intensity-vector for each energy
52 I_a = I(:,1); %all measured intensities for lower energy line (absorbed)
53 I_b = I(:,2); %all measured intensities for higher energy line (non-absorbed)
54
55 if istable(I_a), I_a=table2array(I_a); end %when reading in xlsx-files, Matlab
```

```

stores them as a table. You need to convert them into an array!
56     if istable(I_b), I_b=table2array(I_b); end
57
58 % evaluate the size of I_a for while loop afterwards
59 n = size(I_a);
60
61 %% calculate dose if only current and live time are given
62
63 Ne = 1.602176634*10^(-19);
64 if cur~=1
65     D=cur*tau/Ne;
66 end
67 for k=1:n(1,1)
68 %% quantification: first step without absorption
69 rhot(k)=(zet_a*I_a(k)+zet_b*I_b(k))/D;
70 c_a(k) = zet_a*I_a(k)/(zet_a*I_a(k)+zet_b*I_b(k));
71 c_b(k) = zet_b*I_b(k)/(zet_a*I_a(k)+zet_b*I_b(k));
72
73 %define convergence criteria
74 convconc = 0.001; convrhot = 0.000000000001;
75 convcheck=0;
76
77 %% convergence loop for quantification with absorption correction
78 while convcheck==0
79
80     Abs_a = ((murho_a*c_a(k)+murho_b*c_b(k)) * rhot(k)* csc(degtorad(alpha)))/(1-
exp(-(murho_a*c_a(k)+murho_b*c_b(k)) * rhot(k)* csc(degtorad(alpha))));
81     Abs_b = ((murho_c*c_a(k)+murho_d*c_b(k)) * rhot(k)* csc(degtorad(alpha)))/(1-
exp(-(murho_c*c_a(k)+murho_d*c_b(k)) * rhot(k)* csc(degtorad(alpha))));
82
83     %calculate quantification terms
84     rhottest=(zet_a*I_a(k)*Abs_a+zet_b*I_b(k)*Abs_b)/D;
85     c_atest = zet_a*I_a(k)*Abs_a/(zet_a*I_a(k)*Abs_a+zet_b*I_b(k)*Abs_b);
86     c_bttest = zet_b*I_b(k)*Abs_b/(zet_a*I_a(k)*Abs_a+zet_b*I_b(k)*Abs_b);
87
88     %check convergence
89     delta_ca = abs(c_atest-c_a(k)); % convergence crit: < 0,001wt%
90     delta_cb = abs(c_bttest-c_b(k));
91     delta_rhot = abs(rhottest - rhot(k)); % convergence crit: < 0,01nm
92
93     convcheck=(delta_ca < convconc && delta_cb < convconc && delta_rhot <
convrhot); %check convergence criterion
94
95     c_a(k) = c_atest;
96     c_b(k) = c_bttest;
97     rhot(k) = rhottest;
98
99 end
100 end

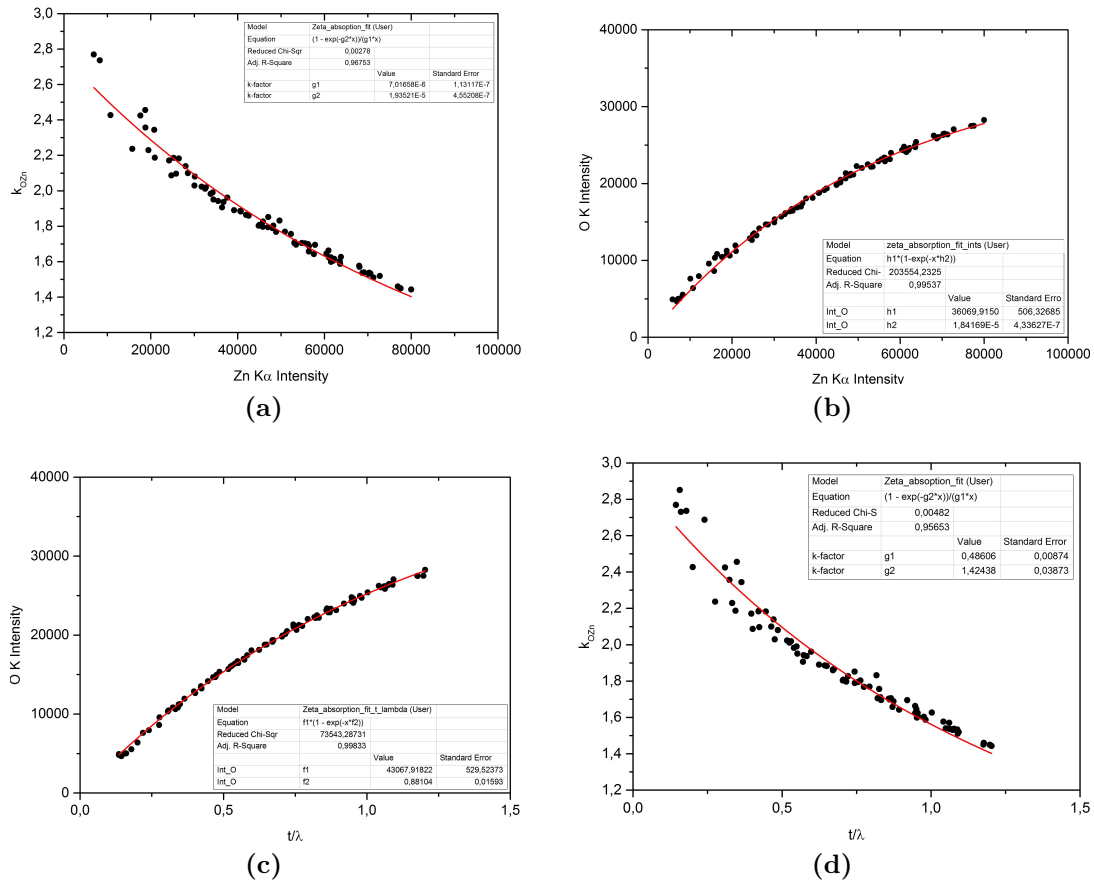
```



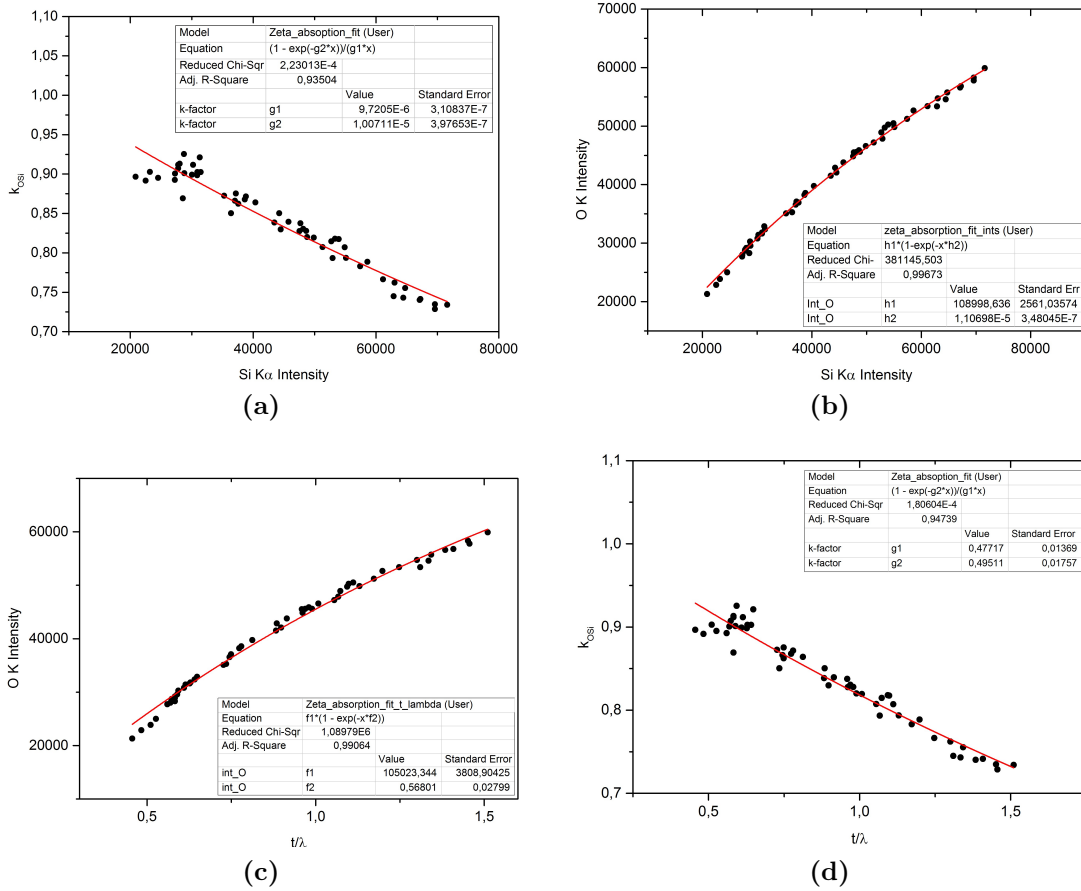
## B Additional graphs

### B.1 Residual graphs for $\zeta$ -factor determination

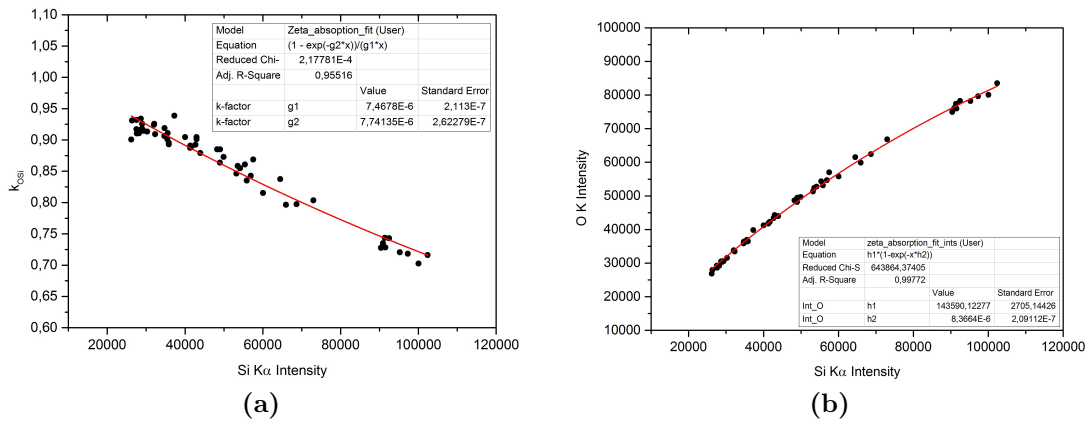
In this section of the appendix all residual graphs for  $\zeta$ -factor determination are illustrated. For each measurement series four graphs have been performed to obtain the fitting parameters of method **A**, **B** and **C**.

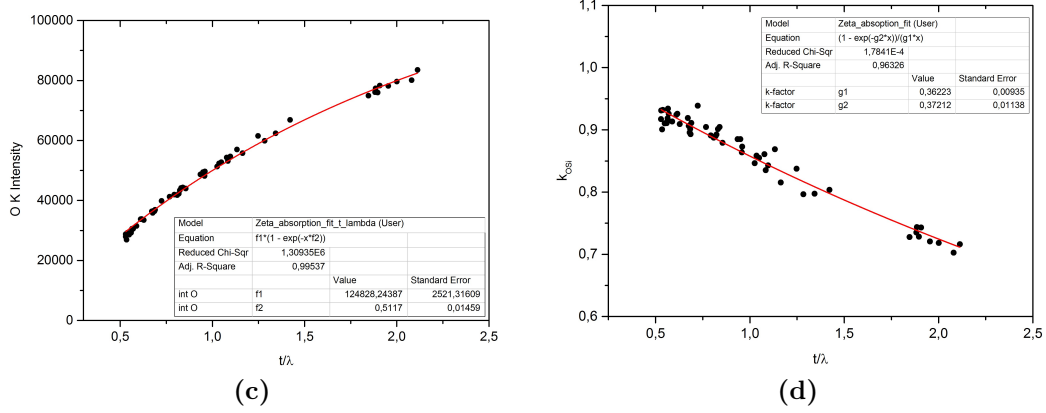


**Figure B.1:** Graphs performed for  $\zeta$ -factor determination of ZnO at detector II; (a) k-factor dependence over Zn K $\alpha$  intensity; (b) O-K intensity dependence over Zn K $\alpha$  intensity; (c) O-K intensity dependence over  $t/\lambda$ ; (d) k-factor dependence over  $t/\lambda$

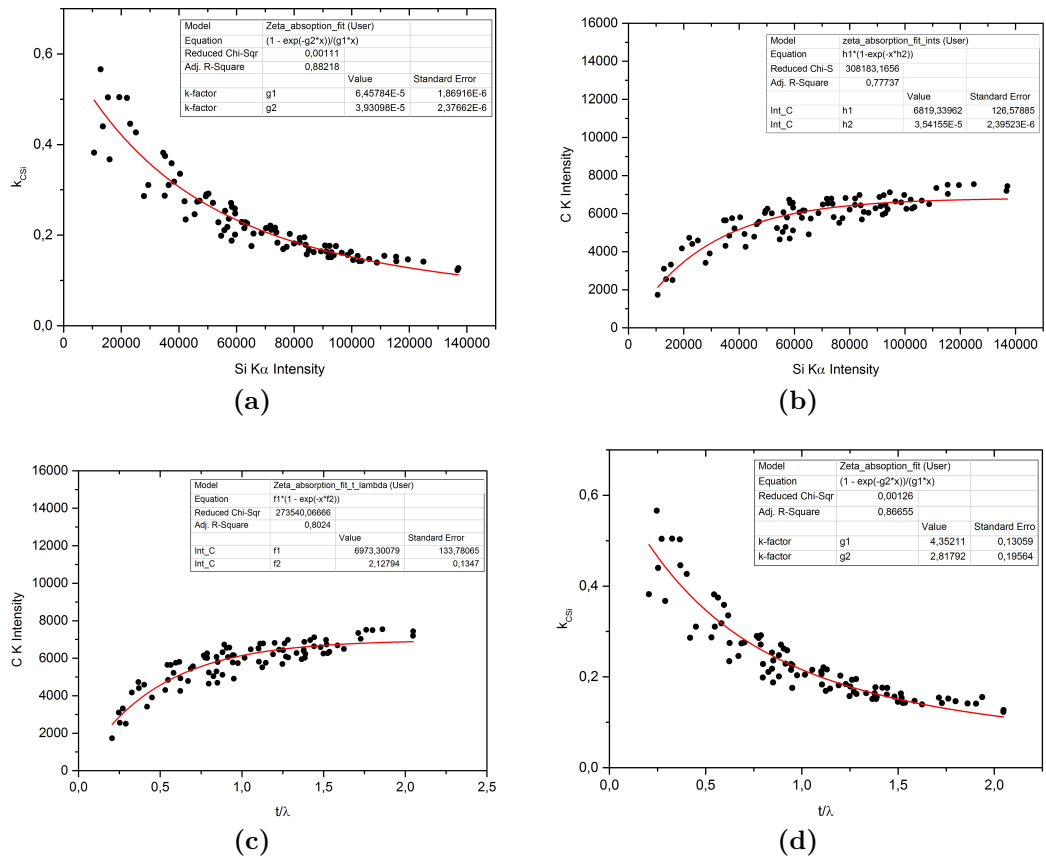


**Figure B.2:** Graphs performed for  $\zeta$ -factor determination of  $\text{SiO}_2$  at detector I; (a) k-factor dependence over Si-K intensity; (b) O-K intensity dependence over Si-K Intensity; (c) O-K intensity dependence over  $\frac{t}{\lambda}$ ; (d) k-factor dependence over  $\frac{t}{\lambda}$

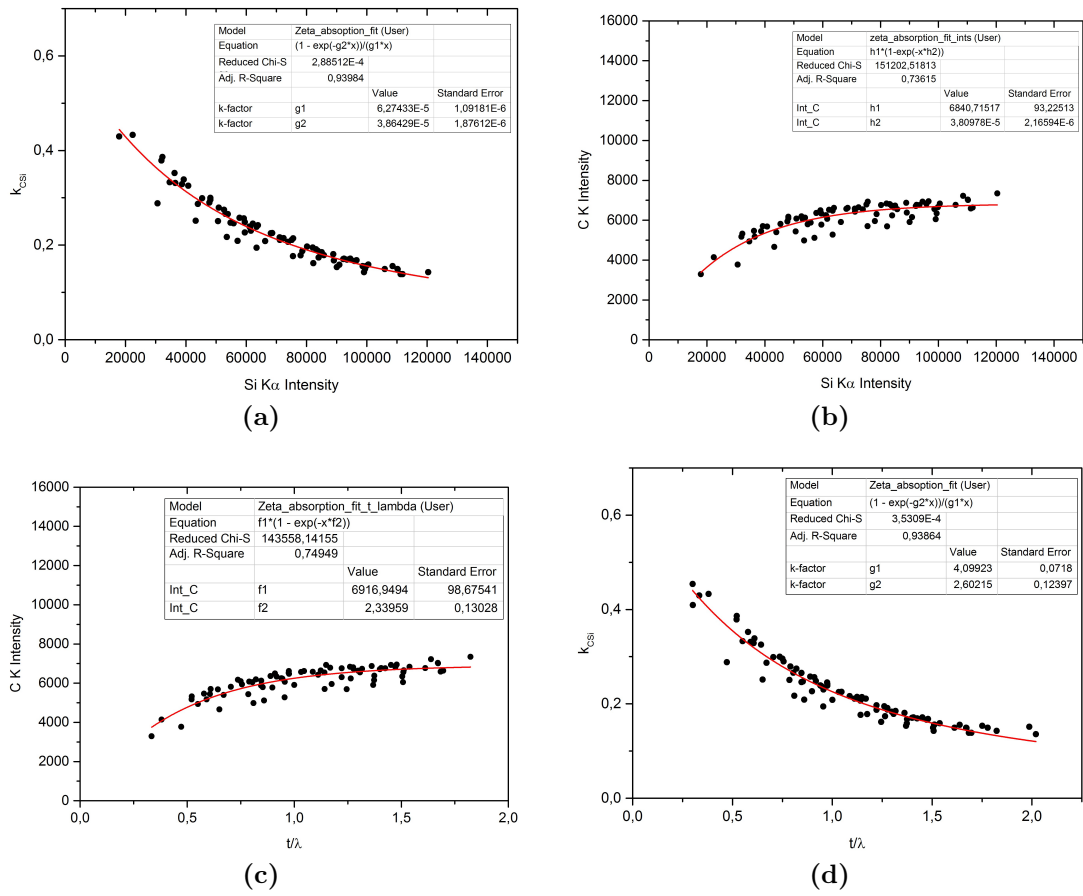




**Figure B.3:** Graphs performed for  $\zeta$ -factor determination of **SiO<sub>2</sub>** at **detector II**; (a) k-factor dependence over Si-K intensity; (b) O-K intensity dependence over Si-K intensity; (c) O-K intensity dependence over  $\frac{t}{\lambda}$ ; (d) k-factor dependence over  $\frac{t}{\lambda}$



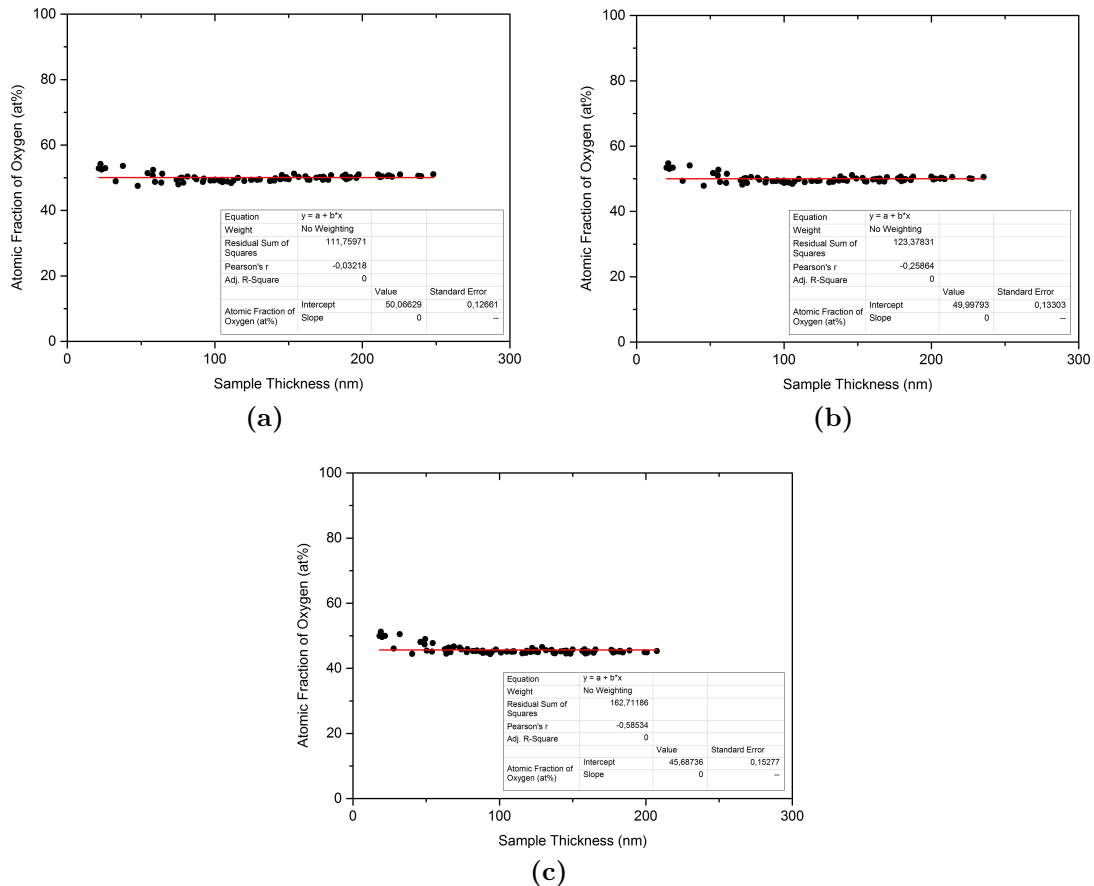
**Figure B.4:** Graphs performed for  $\zeta$ -factor determination of **SiC** at **detector I**; (a) k-factor dependence over Si-K intensity; (b) C-K intensity dependence over Si-K intensity; (c) C-K intensity dependence over  $\frac{t}{\lambda}$ ; (d) k-factor dependence over  $\frac{t}{\lambda}$



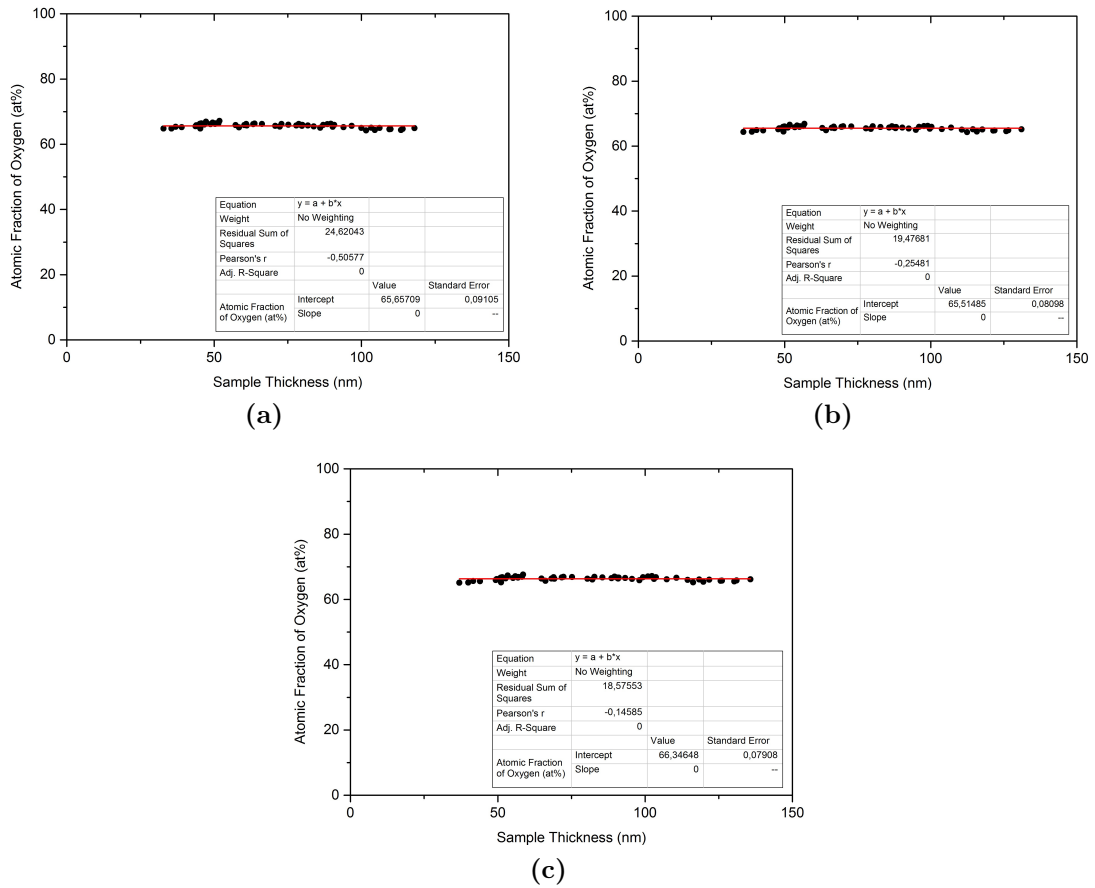
**Figure B.5:** Graphs performed for  $\zeta$ -factor determination of SiC at detector II; (a) k-factor dependence over Si-K intensity; (b) C-K intensity dependence over Si-K intensity; (c) C-K intensity dependence over  $\frac{t}{\lambda}$ ; (d) k-factor dependence over  $\frac{t}{\lambda}$

B.2 Residual graphs of the quantification-procedure via the  $\zeta$ -factor method

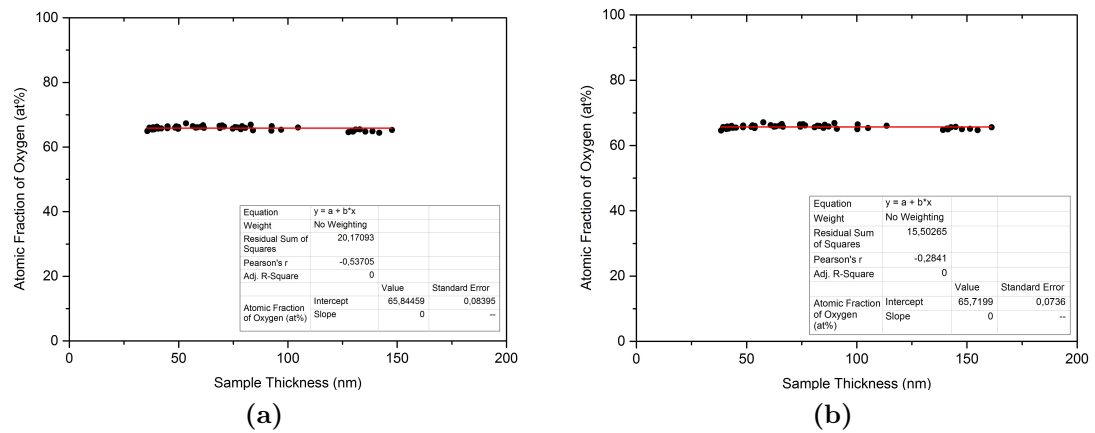
The quantification procedure was performed for every measurement series. The given graphs display the atomic fraction of the light element of the specimen over the absolute specimen thickness. These graphs were made for every method (A, B and C) at each detector.



**Figure B.6:** Determination of the atomic fraction of oxygen in **ZnO**. The intercept of the linear fit indicates the mean value of the elemental concentration in at%. The data was acquired at **detector II** and evaluated with  $\zeta$ -factors obtained by method A (a), B (b) and C (c).



**Figure B.7:** Determination of the atomic fraction of oxygen in  $\text{SiO}_2$ . The intercept of the linear fit indicates the mean value of the elemental concentration in at%. The data was acquired at **detector I** and evaluated with  $\zeta$ -factors obtained by method A (a), B (b) and C (c).



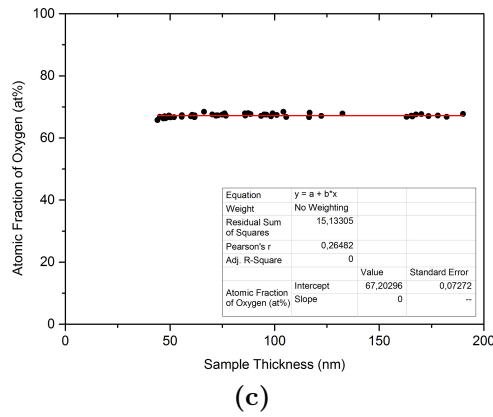


**Figure B.8:** Determination of the atomic fraction of oxygen in  $\text{SiO}_2$ . The intercept of the linear fit indicates the mean value of the elemental concentration in at%. The data was acquired at **detector II** and evaluated with  $\zeta$ -factors obtained by method A (a), B (b) and C (c).

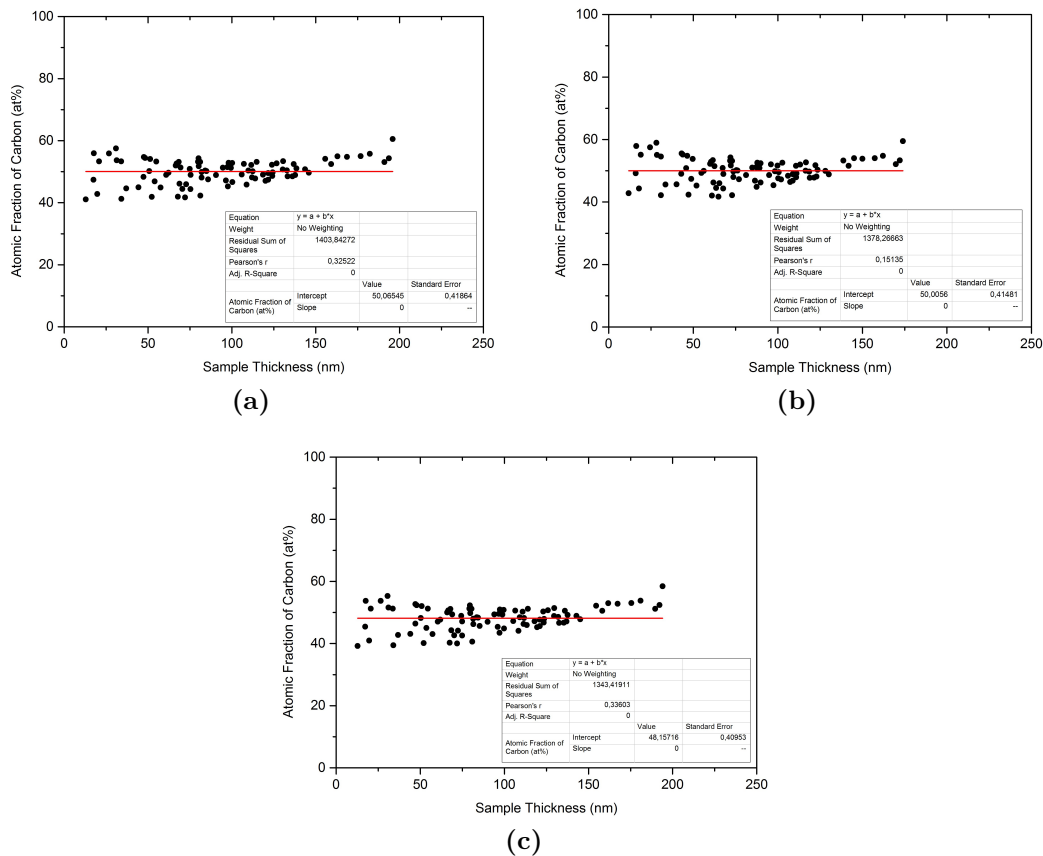


**Figure B.9:** Determination of the atomic fraction of carbon in  $\text{SiC}$ . The intercept of the linear fit indicates the mean value of the elemental concentration in at%. The data was acquired at **detector I** and evaluated with  $\zeta$ -factors obtained by method A (a), B (b) and C (c).

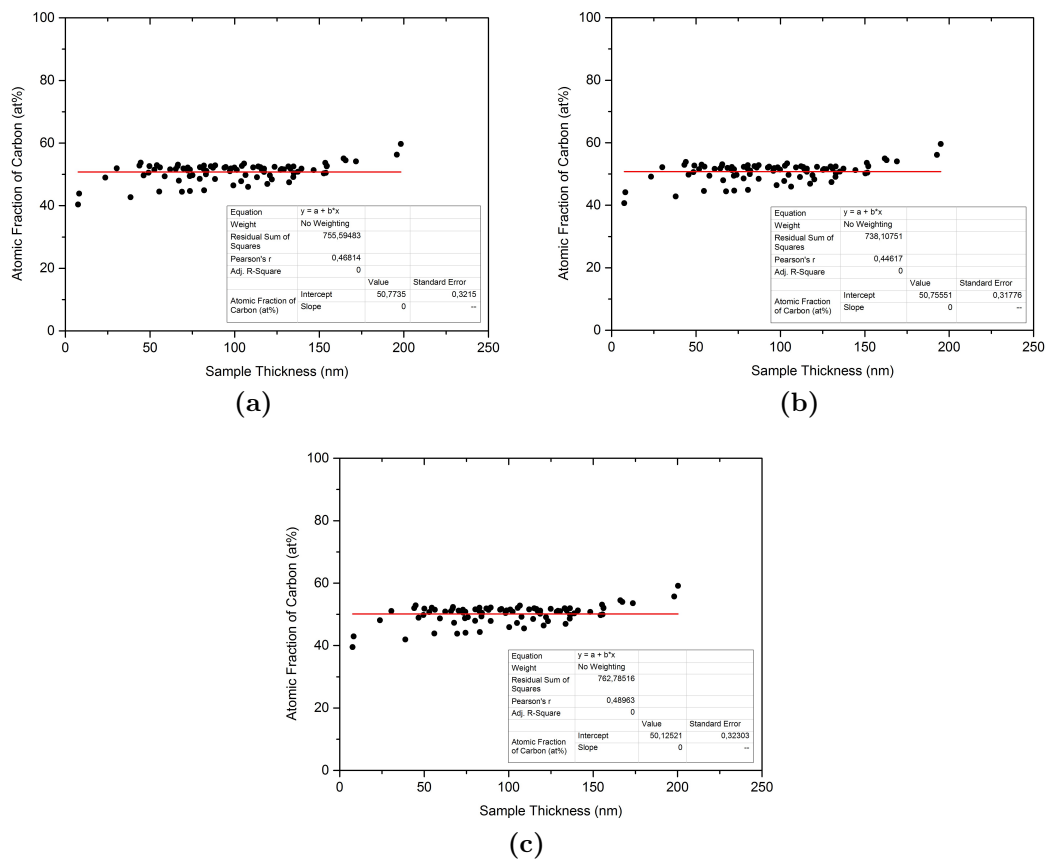


**Figure B.10:** Determination of the atomic fraction of carbon in SiC. The intercept of the linear fit indicates the mean value of the elemental concentration in at%. The data was acquired at **detector II** and evaluated with  $\zeta$ -factors obtained by method A (a), B (b) and C (c).



## C Error analysis

All errors were calculated using single standard deviation. During the fitting procedure the standard error of the fitting parameters is calculated. These values were inserted into the below formulas. The considered error of the electron dose is 1%; the uncertainty of the take-off angle was estimated at  $\pm 0.25^\circ$ .

### Method A

$$\Delta \zeta_A = \left| \frac{c_B D_e \sin \alpha_{TO}}{\sum_i c_i \frac{\mu}{\rho}_i^A} \right| * \Delta g_1 + \left| \frac{g_1 c_B \sin \alpha_{TO}}{\sum_i c_i \frac{\mu}{\rho}_i^A} \right| * \Delta D_e + \left| \frac{g_1 c_B D_e \cos \alpha_{TO}}{\sum_i c_i \frac{\mu}{\rho}_i^A} \right| * \Delta \alpha_{TO} \quad (C.1)$$

$$\Delta \zeta_B = \left| \frac{c_B D_e \sin \alpha_{TO}}{\sum_i c_i \frac{\mu}{\rho}_i^A} \right| * \Delta g_2 + \left| \frac{g_2 c_B \sin \alpha_{TO}}{\sum_i c_i \frac{\mu}{\rho}_i^A} \right| * \Delta D_e + \left| \frac{g_2 c_B D_e \cos \alpha_{TO}}{\sum_i c_i \frac{\mu}{\rho}_i^A} \right| * \Delta \alpha_{TO} \quad (C.2)$$

### Method B

$$\Delta \zeta_A = \left| \frac{c_A D_e \sin \alpha_{TO}}{-h_1^2 \sum_i c_i \frac{\mu}{\rho}_i^A} \right| * \Delta h_1 + \left| \frac{c_A \sin \alpha_{TO}}{h_1 \sum_i c_i \frac{\mu}{\rho}_i^A} \right| * \Delta D_e + \left| \frac{c_A D_e \cos \alpha_{TO}}{h_1 \sum_i c_i \frac{\mu}{\rho}_i^A} \right| * \Delta \alpha_{TO} \quad (C.3)$$

$$\Delta \zeta_B = \left| \frac{c_B D_e \sin \alpha_{TO}}{\sum_i c_i \frac{\mu}{\rho}_i^A} \right| * \Delta h_2 + \left| \frac{h_2 c_B \sin \alpha_{TO}}{\sum_i c_i \frac{\mu}{\rho}_i^A} \right| * \Delta D_e + \left| \frac{h_2 c_B D_e \cos \alpha_{TO}}{\sum_i c_i \frac{\mu}{\rho}_i^A} \right| * \Delta \alpha_{TO} \quad (C.4)$$

### Method C

The  $\zeta$ -factors determined with method **C** depend on the results of two fitting procedures. Therefore, an extra step of error-propagation is needed (see equation C.7).

$$\Delta \zeta_A = \left| \frac{c_A D_e \sin \alpha_{TO}}{-f_1^2 \sum_i c_i \frac{\mu}{\rho}]_i^A} \right| * \Delta f_1 + \left| \frac{c_A \sin \alpha_{TO}}{f_1 \sum_i c_i \frac{\mu}{\rho}]_i^A} \right| * \Delta D_e + \left| \frac{c_A D_e \cos \alpha_{TO}}{h_1 \sum_i c_i \frac{\mu}{\rho}]_i^A} \right| * \Delta \alpha_{TO} \quad (\text{C.5})$$

$$\Delta \zeta_B = |\zeta_A| * \Delta k_{AB} + |k_{AB}| * \Delta \zeta_A \quad (\text{C.6})$$

with

$$\Delta k_{AB} = \left| \frac{1}{l_1} \right| * \Delta g_2 + \left| \frac{1}{-l_2^2} \right| * \Delta g_1 \quad (\text{C.7})$$

$g_1, g_2$ ...fitting parameter of the modified Horita plot (see figure 3.6 d))

$$\Delta \lambda = \left| \frac{\sin \alpha_{TO}}{\rho \sum_i c_i \frac{\mu}{\rho}]_i^A} \right| * \Delta f_2 + \left| \frac{f_2 \cos \alpha_{TO}}{\rho \sum_i c_i \frac{\mu}{\rho}]_i^A} \right| * \Delta \alpha_{TO} \quad (\text{C.8})$$